isvr Institute of Sound and Vibration Research

Design and Development of a Smart Panel with Five Decentralised Control Units for the Reduction of Vibration and Sound Radiation

M. Gavagni, P. Gardonio and C. Galassi

ISVR Technical Memorandum Nº 971

February 2007

University of Southampton

SCIENTIFIC PUBLICATIONS BY THE ISVR

Technical Reports are published to promote timely dissemination of research results by ISVR personnel. This medium permits more detailed presentation than is usually acceptable for scientific journals. Responsibility for both the content and any opinions expressed rests entirely with the author(s).

Technical Memoranda are produced to enable the early or preliminary release of information by ISVR personnel where such release is deemed to the appropriate. Information contained in these memoranda may be incomplete, or form part of a continuing programme; this should be borne in mind when using or quoting from these documents.

Contract Reports are produced to record the results of scientific work carried out for sponsors, under contract. The ISVR treats these reports as confidential to sponsors and does not make them available for general circulation. Individual sponsors may, however, authorize subsequent release of the material.

UNIVERSITY OF SOUTHAMPTON

INSTITUTE OF SOUND AND VIBRATION RESEARCH

SIGNAL PROCESSING AND CONTROL GROUP

Design and Development of a Smart Panel with Five Decentralised Control Units for the Reduction of Vibration and Sound Radiation

by

M. Gavagni, P. Gardonio and C. Galassi

ISVR Technical Memorandum Nº 971

February 2007

Authorized for issue by
Professor R. Allen
Group Chairman

ABSTRACT

This Technical Report discusses the design and the construction of a smart panel with five decentralised direct velocity feedback control units in order to reduce the vibration of the panel dominated by well separated low frequency resonances. Each control unit consists of an accelerometer sensor and a piezoelectric patch strain actuator. The integrated accelerometer signal is fed back to the actuator via a fixed negative control gain. In this way the actuator generates a control excitation proportional and opposite to the measured transverse velocity of the panel so that it produces active damping on the panel. First the open loop frequency response function between the sensor and the actuator of a single channel has been studied and an analogue controller has been designed and tested in order to improve the stability of this control system. Following the stability of all five control units has been assessed using the generalised Nyquist criterion. Finally the performances of the smart panel have been tested with reference to the reduction of the vibrations at the error positions and with reference to the reduction of the radiated sound. Finally in appendix to this Report, a parametric study is presented on the properties of sensor-actuator FRFs measured with different types of piezoelectric patch actuators. The results of this parametric study have been used in order to choose the actuators to be used for the construction of the smart panel.

TABLE OF CONTENTS

1. INTRODUCTION

This Technical Report is concerned with the design and development of a “smart panel” with five independent feedback control units for the implementation of active vibration control (AVC) in order to reduce the response and the sound radiation of the panel [1, 2].

At low frequencies the response of a lightly damped structure is characterised by well separated resonance peaks. Thus the reduction of these peaks allows the reduction of the frequency averaged response of the structure. Resonances are controlled by damping, thus by generating active damping on the structure it is possible to decrease the amplitude of the resonance peaks. A simple and very effective approach for implementing active damping is direct velocity feedback control (DVFB) [3]. In a DVFB control system, the velocity of the structure measured at the control position is fed back to a control actuator via a fixed negative control gain. In this way the actuator generates on the structure a force proportional and opposite to the measured velocity. If the actuator is collocated with the sensor and the control actuation is dual to the velocity sensing (e. g. force-linear velocity or moment-angular velocity) [4], then a sky hook damper is synthesised by the control unit [3]. Active damping can then be efficiently injected in the structure in order to reduce its response and thus sound radiation at the low frequency resonances. The smart panel considered in this Report has five DVFB control units. Each unit is made of a classic accelerometer sensor with an analogue integrator, a voltage amplifier with a compensator circuit and a piezoelectric patch strain actuator.

A critical problem of this control system is the stability both of each feedback loop and the whole set of five control units. A feedback control unit is unconditionally stable if the open loop frequency response function (FRF) between the sensor and the actuator is positive real, i. e. the phase is bound between ±90° [3]. It has been demonstrated that this condition is satisfied if the sensor and the actuator are dual and collocated [4]. The practical DVFB control units considered in this study are neither collocated nor dual. In fact the piezoelectric patch strain actuator generates moments along its edges while the accelerometer sensor with an analogue integrator, measures the transverse velocity of the plate at the centre of the actuator patch. As result the sensor-actuator FRF is characterised by a constant phase lag that brings the FRF to real negative values so that the feedback loop could becomes unstable for high control gains. In fact, according to the Nyquist stability criterion [5, 6], if the locus of the sensor-actuator open loop FRF encircles the Nyquist stability point (-1+j0), then the system is unstable. Even if the locus of the sensor-actuator open loop FRF does not encircles the Nyquist stability point, when the FRF has real negative values, such that it occupies both real negative quadrants of the locus plot, the feedback loop is bound to be only conditionally stable, i. e. only a limited range of feedback control gains can be implemented

before the instability point (-1+j0) is encircled. With the piezo actuator and accelerometer sensor transducers this instability behaviour is magnified by a constant amplitude rise of the sensor-actuator FRF which is due to the piezoelectric actuator bending excitation [7] and by the resonance peak and the correspondent brusque phase change of -180° produced by the accelerometer sensor response [8].

The stability of the control system can be improved firstly by a suitable choice of the accelerometer sensor and piezoelectric patch actuator and secondly by the design of a compensator which corrects the causes of instability. The piezoelectric patch actuator has been chosen in such a way as that, if an ideal massless velocity sensor were to be used, the sensor-actuator open loop FRF is positive real up to about 40 kHz. Also the accelerometer sensor has been chosen with a constant response function up to about 40 kHz where the characteristic resonance of the accelerometer occurs. In this way the accelerometer sensor and piezoelectric patch actuator FRF is bound to be real positive up to about 40 kHz. At higher frequencies the brusque -180° phase shift due to the accelerometer resonance tends to bring the phase beyond -270° so that the frequency band where the open loop sensor-actuator FRF generates instability is diminished. In order to reduce this intrinsic instability it is necessary to design a compensator that rolls off the sensor-actuator FRF above about 35 kHz where the FRF goes real negative. In order to achieve this objective a suitable compensator has been designed and built. The compensator is made of two low pass filters [9] with cut off frequency at 2 kHz and 15 kHz respectively. The first filter reduces the rising effect of the amplitude of the sensor-actuator open loop FRF. The second filter is chosen to further reduce the amplitude of the sensor-actuator response above 35 kHz where instability is generated.

The aim of this Report is to present the design and test study of a smart panel with five independent direct velocity feedback control units which operate all together in order to reduce the vibration and sound radiation of the panel. The study is divided in two steps: firstly the design of a single control unit and improvement of its stability by designing an appropriate compensator and secondly the study of the whole system with five independent control units.

The Report is subdivided in four Sections. Section two describes the structure of the smart panel and in particular its main elements: the aluminium panel, the accelerometer sensors, the piezoelectric actuators and finally the electronic components of the feedback loops. The stability of one control unit is analysed in Section three. The selection of the piezoelectric actuator is based on a parametric experimental study carried out with three sets of actuators with circular, square and rectangular shapes and various dimensions, which is summarised in Appendix 1. This study continues by presenting the design and the construction of an analogue compensator in order to improve the stability of the control unit. The Section ends with the stability analysis of the five

control units when used at the same time. Finally Section four describes the control performances of the smart panel in terms of the measured transverse velocity at the error positions and the measured sound pressure level generated by the panel at a point 0.5 m above the centre of the panel.

2. DESCRIPTION OF THE SYSTEM

The object of this Section is to describe the components of the smart panel. Firstly the mechanical structure of the panel will be described. Secondly the physical and dynamics properties of the seismic accelerometer sensors and of the piezoelectric patch strain actuators will be discussed. Finally, in order to complete the description of the control chain, the electronic components, that is the analogue integrator and the high voltage amplifier, will be described.

2.1 Smart panel

The prototype smart panel is made by aluminium plate of thickness h_p = 1 mm which has been fixed on a rigid frame so that the vibrating area is $l_x \times l_y$ = 414×314 mm^2. The physical and geometric properties of the panel are summarised in the table below.

Table 1 Dimensions and physical properties of the thin aluminium plate.

Parameter	**Value**
Length	l_x=474 mm
Width	l_y=374 mm
Thickness	h_p=1 mm
Density	ρ=2700 kg/m^3
Poisson's ratio	η=0.05
Young's modulus	E=7×10^{-10} N/m^2

Five accelerometer sensors are fixed on the top side of the panel while on the bottom side, in correspondence of the sensors, are bonded five piezoelectric patch strain actuators. These sensor-actuator pairs are arranged in a "cross geometry" as shown in Figures 1 and 2. Their positions have been chosen in such a way as to avoid the nodal lines of the low order modes of the plate where the transverse velocity of the structure is zero or very small so that the feedback signals, and then the control authorities of the systems, would be very low at resonances controlled by these low order modes.

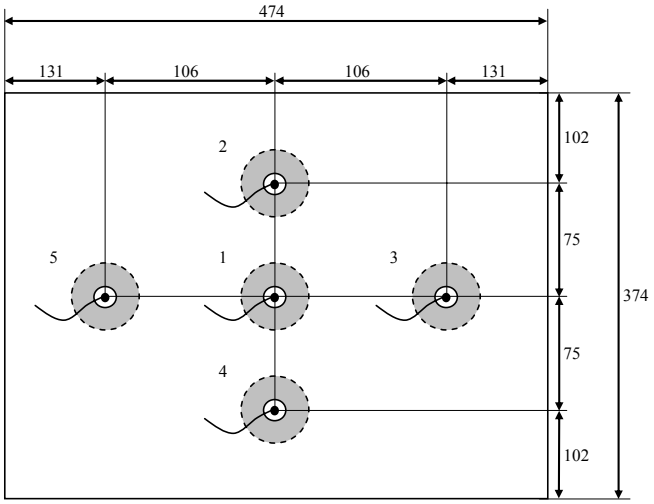

Fig. 1 Panel with five sensor-actuator pairs. The sensors are placed on the top of the panel and the actuators, are bonded on the bottom of the panel in correspondence of the sensors. The positions of the control units and the dimensions of the plate are expressed in mm.

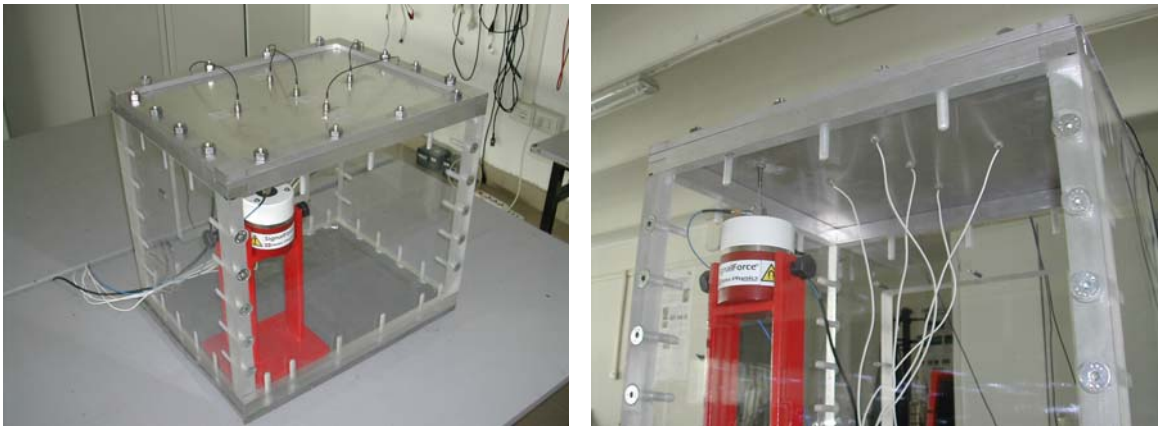

Fig. 2 Prototype of smart panel formed by a thin aluminium plate and five decentralized feedback control units.

2.2 Piezoelectric patch strain actuator

As discussed in Reference 10, the choice of the sensor and actuator transducers is very important because these elements affect the stability of the control loops. The actuator chosen for this study is a piezoelectric patch strain actuator. Piezoelectric actuators are devices that produce small strain deformation with an high stress capability for a given driving voltage. In order to generate bending vibration on the panel, thin patches are bonded on the surface of the panel, as shown in Figures 1 and 2. The strain deformation of the patch generates in plane strain on the surface of the panel which therefore produces bending deformation of the whole panel. Piezoelectric patch actuators have many properties for their use in vibration control systems: wide frequency linear response, high control forces without the necessity to interact with other structures apart from the panel, low weight, low cost. In order to obtain an unconditionally stable feedback control loop, as discussed in Section 1, the sensor-actuator pair must be dual and collocated. As discussed in Reference 10, a sensor-actuator pair made of an accelerometer and a piezoelectric patch strain actuator is neither

dual nor collocated so that the control unit is not unconditionally stable. In order to reduce the intrinsic instability of this control system, the physical and geometric properties of the piezoelectric actuator should be selected in such a way as the open loop sensor-actuator FRF is positive real in the whole frequency band where the control is desired and it rolls off above this frequency band so that the real negative part of the FRF has much smaller amplitude than the real positive part.

For this purpose an experimental parametric study (see Appendix 1) has been carried out using a large number of piezoelectric actuators, which are made of a typical piezoelectric material whose characteristics are summarised in Table 2 below.

Table 2: Physical properties of the piezoelectric patch strain actuators.

Parameter	Value
Density	ρ=7800 kg/m^3
Strain constant	d_{31}=183×10^{-12} m/V
Poisson ratio	ν_p=0.35

The experimental parametric study has been carried out by measuring the frequency response function between the transverse velocity of a plate at the control position and the input voltage to the piezoelectric patch strain actuators bonded to the plate. As shown in Figure 3, the transverse velocity has been measured by a laser vibrometer in order to leave out the dynamic effects of a practical sensor, such as a seismic accelerometer. Also the piezoelectric patch actuator has been driven by a high voltage amplifier.

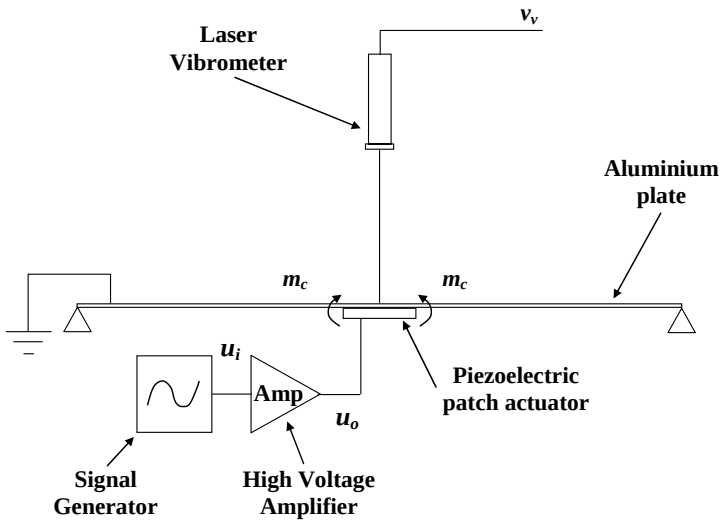

Fig. 3 Aluminium plate excited in bending by a piezoelectric patch strain actuator bonded on the bottom side. The actuator is driven by the output signal, u_o, of an high voltage amplifier and the transverse velocity, v_v, of the plate is measured by a laser vibrometer.

The actuators considered in the parametric study have been divided in two groups. The first group contains samples of different shapes (squared, rectangular and circular), with fixed thickness (1

mm) and different dimensions and masses. The second group contains samples of different shapes (squared, rectangular and circular), with fixed mass (5 g) and different dimensions and thicknesses. In total the open loop FRF measured with 21 actuators have been studied. In this way it has been possible to estimate the influence of shape, dimensions and mass of the piezoelectric actuator on the open loop FRF with a massless velocity sensor. Only the main results and conclusions are presented in this Subsection. The whole set of measurements is presented in Appendix 1 in terms of Bode and Nyquist plots of the measured open loop FRFs. The study has shown that the increase of the dimensions of the piezoelectric patch determines an increase of the amplitude of the FRF, although at the same time it also determines an increase of the phase lag effect. Thus with an ideal velocity sensor such as the laser vibrometer, actuators with small dimensions strongly contribute to the stability of the control system. This result is probably due to the fact that smaller is the size of the actuator the greater is the collocation between sensor and bending actuation around the perimeter of the patch. However, actuators characterised by small size are not able to generate high strain before saturation occurs and the actuation strength becomes non linear. Thus they cannot produce high control strengths. Finally the study has shown that the shape influences in a limited way the open loop sensor-actuator FRF although circular actuators have shown slightly better stability properties than the quadrilateral ones.

Taking into account the results obtained from the parametric study, it has been chosen to use an actuator with intermediate size which offers the best trade off between the actuation strength and the phase lag effect. The geometric properties of the chosen actuator are summarised in Table 3.

Table 3: Geometric properties of the piezoelectric actuator chosen in order to build the smart panel.

Parameter	**Value**
Shape	Circular
Diameter	d=21.00 mm
Thickness	h=1.98

The pictures in Figure 4 show the size and bonding of the piezoelectric actuator to the plate. The chosen piezoelectric actuator is rather small and light so that it does not affect significantly the dynamic behaviour of the panel.

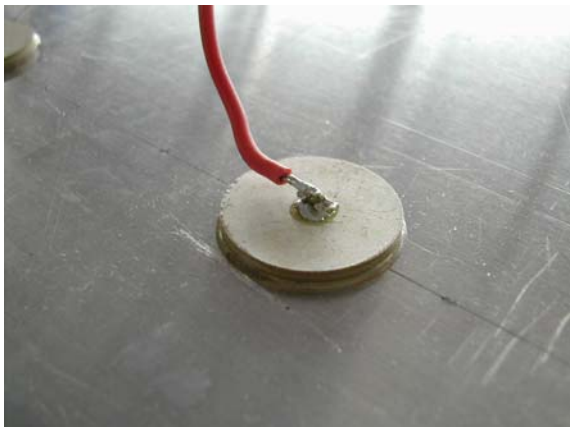

Fig. 4 The piezoelectric patch strain actuator bonded to the panel at the control position number 2.

Figures 4 show the Bode and the Nyquist plots of the open loop FRF of the piezoelectric patch strain actuator attached on the panel at the control position number 2. The open loop frequency response function G is given by the ratio between the output signal of the laser vibrometer, v_v, and the input voltage to the piezoelectric patch actuator, u_o, i. e the output signal of the amplifier which drives the piezoelectric patch actuator.

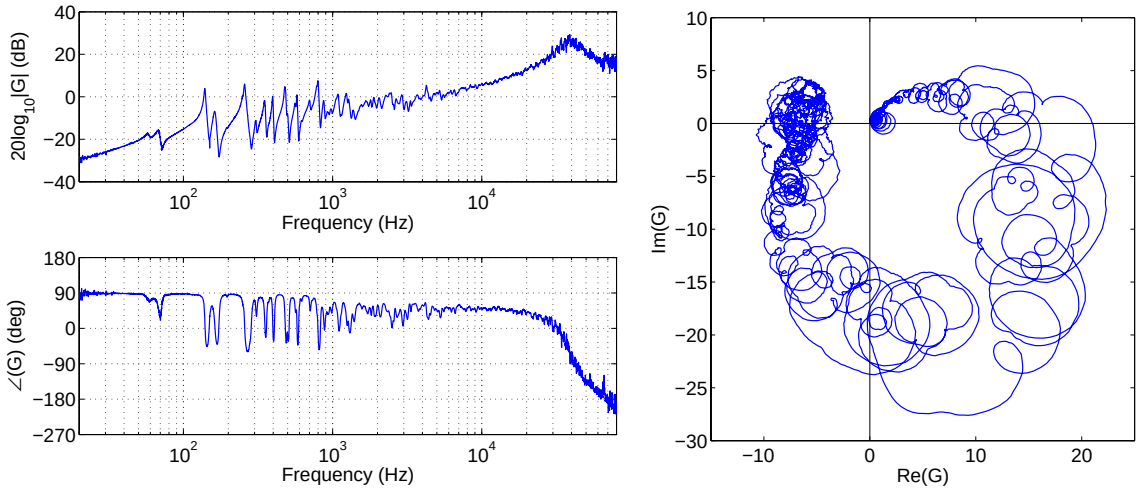

Fig. 5: Bode plot (left hand side) and Nyquist plot (right hand side) of the open loop frequency response function between the output signal v_v of the laser vibrometer and the input signal u to the piezoelectric patch strain actuator bonded at the control position number 2 of the panel.

The Bode plot highlights the two characteristic features of piezoelectric actuation: first, the response amplitude increases monotonically with frequency and second, the phase rolls off monotonically with frequency. In particular the phase exceeds -90° at about 40 kHz. Thus even if a nearly ideal velocity sensor, as the laser vibrometer, is used, a feedback loop with this actuator is only conditionally stable. This is confirmed by the Nyquist plot in Figure 5 which shows that the locus of the FRF enters the left hand side quadrants so that, when high feedback control gains are implemented, the locus can encircle the Nyquist instability point (-1+j0). Of particular interest is the

wide band smooth peak of the sensor-actuator FRF between 35 kHz and 45 kHz. Its origin is not entirely clear. The parametric study has highlighted that it depends on the size of the actuator and for the largest size considered in the study two of these wide band peaks appear in the frequency band up to 80 kHz.

2.3 Accelerometer sensor

The sensor chosen for this study is a classic seismic accelerometer which is the best solution for the practical construction of a DVFB with the piezo patch actuator. This type of sensor is characterised by a wide frequency linear response, high sensitivity and low weight as shown in Figure 6. An accelerometer sensor can be modelled [11] by a seismic mass m_a connected to the vibrating case via a spring of stiffness k_a and a dashpot of damping coefficient c_a.

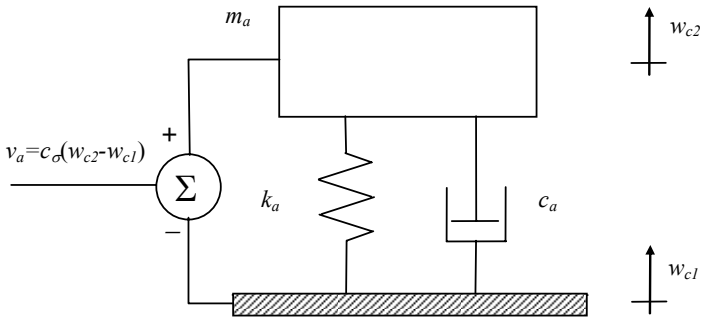

Fig. 6. Schematic representation of an accelerometer transducer made of a seismic mass m_a, which is suspended on the vibrating base via a spring, of stiffness k_a, and a damper with damping coefficient c_a.

In a commercial accelerometer the spring is a piezoelectric transducer which is the active element of the sensor. When the accelerometer is subjected to vibrations, a force, which acts on the piezoelectric element, is generated. According to Newton's law this force is equal to the product of the acceleration and the seismic mass. The piezoelectric effect produces a charge output proportional to the force applied to it. Thus, since the seismic mass is constant, the charge output signal, generated by the piezoelectric material, is proportional to the acceleration of the mass. From literature, the frequency response function of an accelerometer sensor is [11]:

$$H(\Omega) = \frac{-\frac{1}{\omega_a^2}}{(1-\Omega^2) + j2\zeta_a\Omega}, \tag{2.3.1}$$

where $\omega_a = \sqrt{\frac{k_a}{m_a}}$ is the natural frequency of the accelerometer, $\Omega = \frac{\omega}{\omega_a}$ is the normalised frequency and $\zeta_a = \frac{c_a}{2\sqrt{k_a m_a}}$ is the damping ratio of the accelerometer. Figure 7 shows the Bode plot of the frequency response function between the output signal of an accelerometer sensor, v_a, and the acceleration of the base, $-\omega^2 w_{c1}$, calculated using Equation 2.3.1.

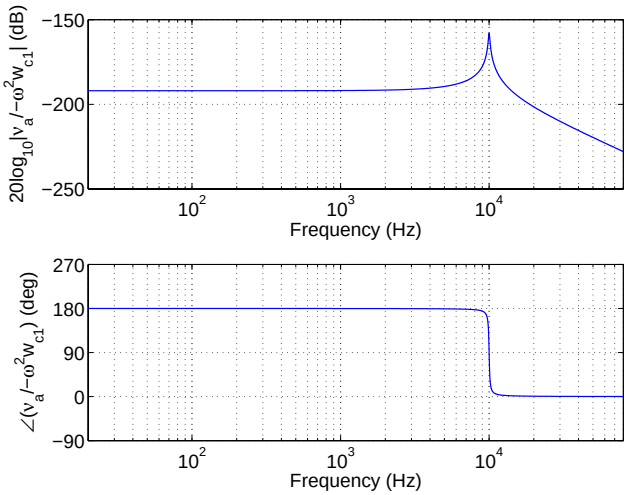

Fig. 7: Amplitude (top plot) and phase (bottom plot) of the simulated frequency response function of an accelerometer sensor.

Equation 2.3.1 and Figure 7 show two important properties of an accelerometer: firstly it can be regarded as a mechanical low pass filter with a resonance peak and a correspondent abrupt phase change of -180° at $\omega = \omega_a$; secondly below this resonance frequency, the sensitivity of the sensor, i. e. output signal per unit base acceleration, is inversely proportional to the squared resonance frequency. In order to achieve a wider operating frequency band the resonance frequency should be rather high but this choice decreases the sensitivity of the sensor.

This dynamic behaviour suggests that, in order to build a DVFB control unit with good stability and performance properties it is necessary to choose an accelerometer sensor whose resonance frequency corresponds to the desired upper frequency limit. In this way the amplitude roll off above this resonance frequency should contribute to lessen the instability effect produced by the phase lag effect due to the non collocation with the piezoelectric patch actuator. This type of conclusion has to be mediated with a possible problem which could be originated by the 180° phase lag introduced by the resonance of the accelerometer. Also the abrupt increase of response at the accelerometer resonance frequency should be carefully taken into account since it could be a principal cause of instability if the non collocation between the piezoelectric actuator and the accelerometer sensor has

produced a phase lag of about -90° at the resonance frequency of the accelerometer. As discussed in Subsection 2.2, the phase of the open loop ideal velocity sensor and chosen piezoelectric patch actuator FRF exceeds -90° at about 40 kHz. The accelerometer sensor should therefore be chosen in such a way as its resonance is well above 40 kHz so that the resonance peak occurs at a frequency where the phase lag of the sensor-actuator FRF exceeds 360° and thus does not affect stability.

The characteristics of the commercial accelerometer sensor (Metra Mess model KS94.100 with ICP® compatible output) chosen to build the single DVFB control units are summarised in the Table below and the accelerometer is represented in Figure 8.

Table 4: Physical properties of the accelerometer sensor.

Parameter	Value
Mass of the accelerometer case	3.5 g
Sensitivity	14 mV/g
Measuring range	±60 g
Resonance frequency	$f_n \approx 45$ kHz

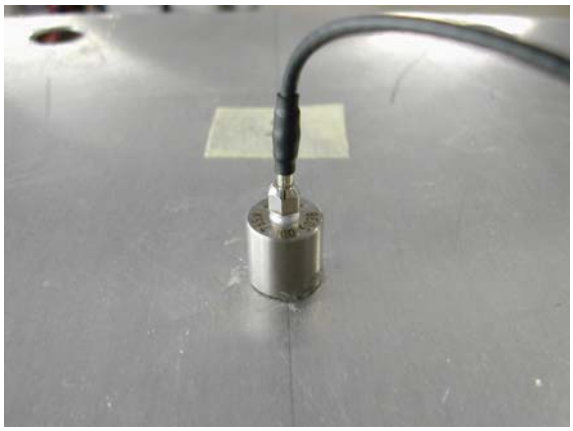

Fig. 8 The accelerometer sensor attached on the panel at the control position number 2.

2.4 Analogue control system

As discussed in Section 1, the control strategy to be implemented is a DVFB loop. Using this architecture and the sensor-actuator pair previously described, the main elements of an analogue control system for such a control unit is made of an integrator circuit, a high voltage amplifier and a compensator. The compensator circuit will be described in next Section where the control system stability is analysed.

In order to implement a direct velocity feedback control loop it is necessary to measure the transverse velocity of the plate. For this purpose an analogue integrator has been put in series to the accelerometer sensor. Figure 9 shows the electrical scheme of the active integrator circuit used in this study.

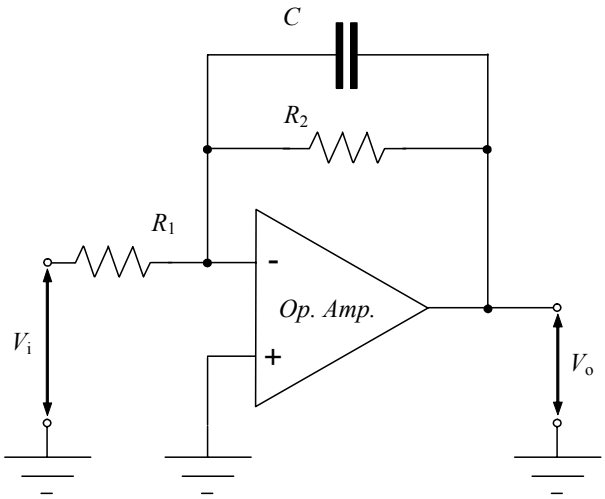

Fig. 9 Electrical scheme of an active integrator circuit.

A classic integrator circuit has a very low amplitude output signal V_o because the integrator operates as a low pass filter. In order to magnify the output signal from the integrator an operational amplifier can be used. An operational amplifier, normally referred to as an "op-amp" for brevity, is a DC-coupled high-gain electronic voltage amplifier with differential inputs and, usually, a single output. In its ordinary operation, the output of the op-amp is controlled by negative feedback which, because of the high gain of the amplifier, determines the level of the output voltage for any given input. The frequency response function of this electrical circuit, that is the ratio between the output signal, V_o, and the input signal, V_i, is given by

$$\frac{V_o}{V_i} = \frac{-\frac{R_2}{R_1}}{1 + j\omega\tau}, \tag{2.4.1}$$

where

$$\tau = R_2 C \tag{2.4.2}$$

is called the time constant of the integrator and R_1, R_2, C are the resistances and the capacitance of the elements in the integrator circuit in Figure 9. The time constant τ sets the cut off frequency of the integrator, that is the lower frequency at which the circuit starts to integrate the input signal:

$$f_c = \frac{\omega_c}{2\pi} = \frac{1}{2\pi\tau} = \frac{1}{2\pi R_2 C}. \tag{2.4.3}$$

As Equation 2.4.1 shows, the frequency response function of the circuit is similar to the response function of a classic passive integrator but it is multiplied by a factor $-R_2 / R_1$. The negative sign takes into account that the integrator, shown in Figure 9, produces a phase change of 180° in order to make the measured velocity suitable for a negative feedback control loop. Table 5 summarises the properties of the electrical elements of the integrator circuit considered in this study.

Table 5: Values of the electrical elements of the integrator circuit.

Parameter	Value
Operational amplifier	OPA131
R_1	1 kΩ
R_2	150 kΩ
C	1.35 μF
f_c	0.786 Hz

The plots in Figure 10 below show a comparison between the simulated FRF and the measured FRF of the integrator. An ideal integrator circuit should produce a $\frac{1}{\omega}$ constant amplitude roll off and a -90° phase at frequencies above the cut-off frequency f_c, which in this case is 0.786 Hz. The circuit built for this study obtains this result at about 20 Hz and progressively it stops to operate for frequencies higher than 4 kHz, because of the non perfect behaviour at these frequencies of the electrical components of the analogue circuit.

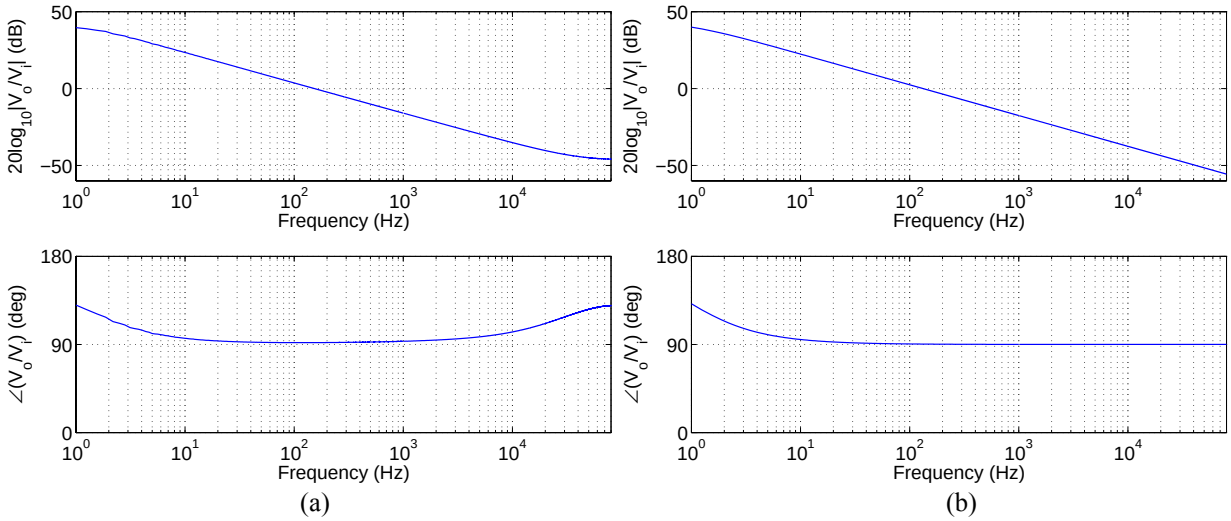

Fig. 10: Amplitude (top plots) and phase (bottom plots) of the integrator frequency response function: a) measured FRF, b) simulated FRF.

The other principal electric component of the feedback loop is the high voltage amplifier which drives the piezoelectric actuator. As shown in Figure 11, a five channels high voltage amplifier has been used in this study. Each channel has a fixed gain (×20), featuring ±200 V (400 V peak to peak) output. Each channel accepts a maximum input voltage of ±10 V.

Fig. 11: High voltage amplifier with five independent channels and fixed gain.

This equipment is output protected from short circuits and has an automatic offset compensator. It is especially suited to drive piezoelectric transducers. The high voltage amplifier is equipped with an external preamplifier stage (shown in Figure 12) with five independent channels and programmable gains. The preamplifier allows four level of preamplification for different maximum input voltage: 1) ±10 V (×1), 2) ±1 V (×10), 3) ±100 mV (×100) and 4) ±10 mV (×100).

Fig. 12: External preamplifier with five independent channels and programmable gains.

Figure 13 shows the measured frequency response function of the channel number 2 of the high voltage amplifier when the gain in the preamplifier is set to ×10 with an input signal amplitude of ±1 V.

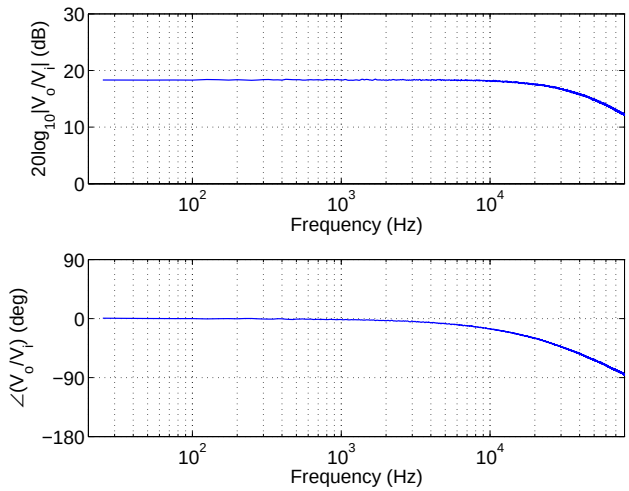

Figure 13: Amplitude (top plot) and phase (bottom plot) of the measured frequency response function of the high voltage amplifier.

Above about 15 kHz, the amplitude and phase of the FRF decrease monotonically. The phase lag could influence the stability of the control unit but this undesired effect is balanced by the amplitude roll off. The electronic chain of the control system is completed by a five channels ICP® converter which feeds the ICP® accelerometer sensors.

2.5 Testing facility

In order to carry out the measurements on the smart panel and to test its performances, the panel has been fixed on an aluminium frame which is mounted on a rectangular cavity made of plexiglass. The panel has been excited by a point force generated by a shaker which, as shown in Figure 2, is mounted inside the box. A scheme of this testing facility is shown in Figure 14.

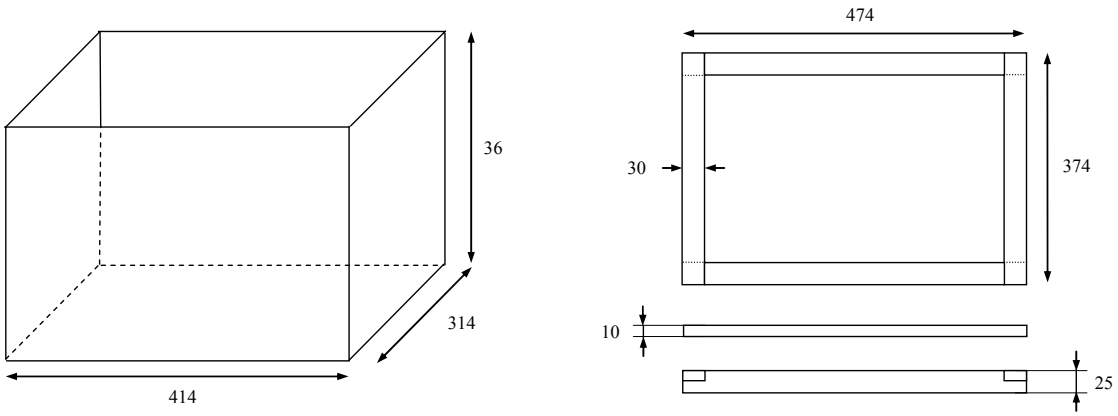

Fig. 14: Schematic of the rectangular cavity (box) made of plexiglass (left hand side) and rigid aluminium frame used in order to clamp the smart panel to the box (right hand side). The dimensions of the cavity and of the frame are expressed in mm.

The thickness of the walls of the box is 30 mm. In this way it is possible to reduce the sound irradiated outside of the cavity through the walls and then it is possible to measure the sound generated by the top face of the panel with and without the control.

3. STABILITY ANALYSIS AND DESIGN OF FIVE DVFB CONTROL UNITS

This Section presents the stability study: firstly of one DVFB control unit and secondly of the whole set of five decentralised control units. Subsection 3.1 describes the type of compensator used in order to improve the stability of the DVFB control loop, while Subsection 3.2 analyses the stability of five control units using the Nyquist criterion for Multiple Input Multiple Output (MIMO) feedback control systems.

3.1 Stability analysis and design of a single control unit

Figure 15 below shows the block diagram of the direct velocity feedback control loop implemented in the smart panel considered in this Report.

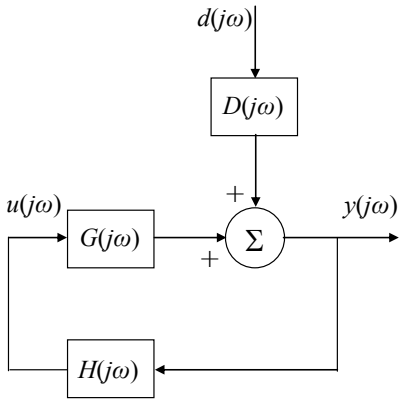

Fig. 15: Block diagram of a single direct velocity feedback (DVFB) control loop.

The output signal from the control sensor $y(j\omega)$ is the superposition of the signals generated by the vibrations of the panel due to the external primary disturbance $d(j\omega)$ and the excitation generated by the piezoelectric actuator, which is proportional and opposite to the accelerometer output signal. Thus the ratio between the error signal $y(j\omega)$ and the primary disturbance is given by:

$$\frac{y(j\omega)}{d(j\omega)} = \frac{D(j\omega)}{\left[1 + G(j\omega)H(j\omega)\right]}, \tag{3.1.1}$$

where $G(j\omega)$ is the open loop frequency response function between the control sensor and the control actuator, $D(j\omega)$ is the frequency response function between the control sensor and the primary disturbance and $H(j\omega)$ is the control function which, in the ideal case, is given by the integrator response function multiplied by a constant gain. As described in the previous Sections, the control system under study is not unconditionally stable. The Bode and Nyquist plots in Figure

5 show that, even if the response of the accelerometer sensor (see Figure 7), of the analogue integrator (see Figure 10) and of the high voltage amplifier (see Figure 13) are not taken into account, the open loop frequency response function of the control system is only conditionally stable. Moreover the size of the positive real part of the plot is comparable to that of the real negative part. Thus relatively low control effects can be produced even when the maximum feedback gain is implemented. Figure 16 below shows the measurement setup when all the components of the control chain are taken into account. Figure 17 shows the Bode and Nyquist plots of the open loop FRF between the output signal v_i of the analogue integrator and the input signal u_i to the high voltage amplifier. Thus these Bode and Nyquist plots represent the open loop frequency response function $G(j\omega)$ $H(j\omega)$ of the complete feedback control system.

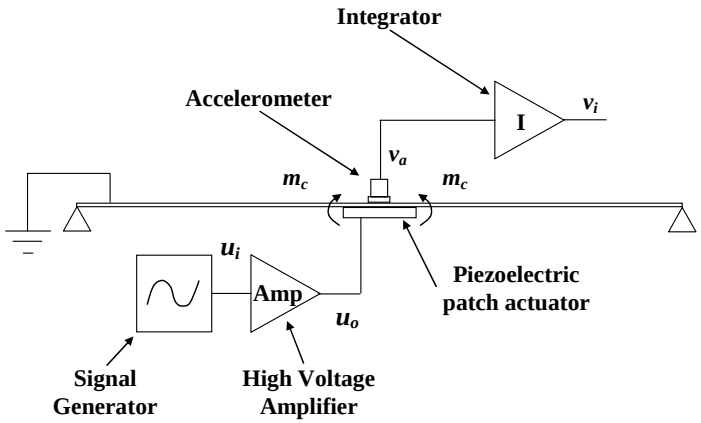

Fig. 16 Aluminium plate excited in bending by a piezoelectric patch strain actuator bonded to the plate. The actuator is driven by the output signal, u_o, of an high voltage amplifier and the transverse velocity, v_i, of the plate is measured by an accelerometer sensor with an analogue integrator circuit in cascade.

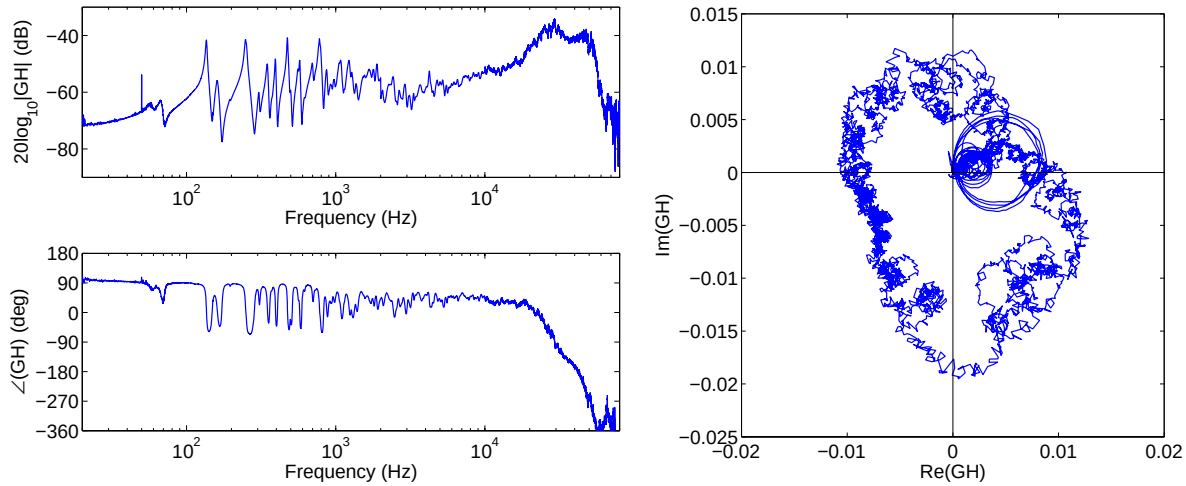

Fig. 17: Bode plot (left hand side) and Nyquist plot (right hand side) of the open loop frequency response function between the output signal of the analogue integrator in series with the accelerometer sensor and the input signal to the high voltage amplifier which drives the piezoelectric patch strain actuator bonded at the control point 2 of the panel.

Comparing these Bode and Nyquist plots with those ones in Figure 5 it is possible to highlights four important characteristics of the system: first at about 50 kHz, there is a new resonance peak and a

phase change of -180° due to the sensor resonance; second the open loop FRF exceeds -90° at 30 kHz; third the locus makes a full circle and returns in the real-positive half plane; fourth the maximum amplitudes of the positive real part and that of the negative real part are still about the same. In conclusion the control system is conditionally stable and very low control performances are predicted [8].

In order to improve the performance of the feedback loop it is necessary to reduce the amplitude of the real negative part of the open loop FRF. This can be obtained by filtering the analogue integrator output signal with a low pass filter [9]. Figure 18 shows the scheme of a second order Sallen-Key low pass filter that has been considered in this work.

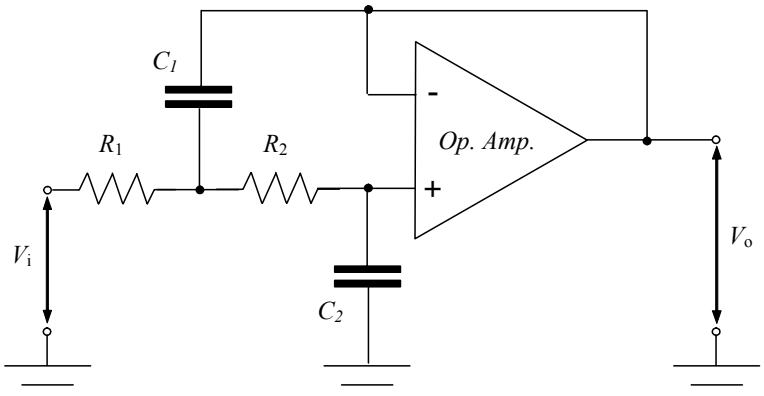

Fig. 18: Electrical scheme of a second order Sallen-Key low pass filter circuit.

A Sallen-Key filter is particularly valued for its simplicity. The circuit in the low pass configuration, produces a second order (2-pole) response which is characterised by a constant amplitude reduction of 12 dB/octave. The operational amplifier is used as a buffer. In this way higher order filters can be obtained by cascading two or more stages. The frequency response function of this filter is given by:

$$\frac{V_o}{V_i} = \frac{\omega_0^2}{-\omega^2 + j\omega\left(\frac{1}{R_2 C_1} + \frac{1}{R_1 C_1}\right) + \omega_0^2}, \tag{3.1.2}$$

where ω_0 is the circular cut off frequency given by

$$\omega_0 = \sqrt{\frac{1}{R_1 R_2 C_1 C_2}}. \tag{3.1.3}$$

The best frequency profile of the filter response function has been derived with a trial and error iterative simulation process where the capacitors and resistors have been varied within the practical

limits of commercial components. Two second order Sallen-Key low pass filters with different cut off frequencies, 5.305 kHz and 15.915 kHz respectively, have been put in cascade. Tables 6 and 7 summarise the electrical components of the two low pass filters built for this study.

Table 6: Values of the electrical elements for the first low pass filter circuit.

Parameter	Value
Operational amplifier	OPA131
R_1	3 kΩ
R_2	3 kΩ
C_1	10 nF
C_2	10 nF
f_c	5.305 kHz

Table 7: Values of the electrical elements for the second low pass filter circuit.

Parameter	Value
Operational amplifier	OPA131
R_1	1 kΩ
R_2	1 kΩ
C_1	10 nF
C_2	10 nF
f_c	15.915 kHz

The comparison between the measured and simulated frequency response function of the two low pass filters in cascade is shown in Figure 19 below. The two plots show that the analogue circuit response is very close to the predicted one. In particular the Bode plot highlights that, as expected, the amplitude reduction is about 24 dB/octave and that the phase lag is about -360° at high frequency.

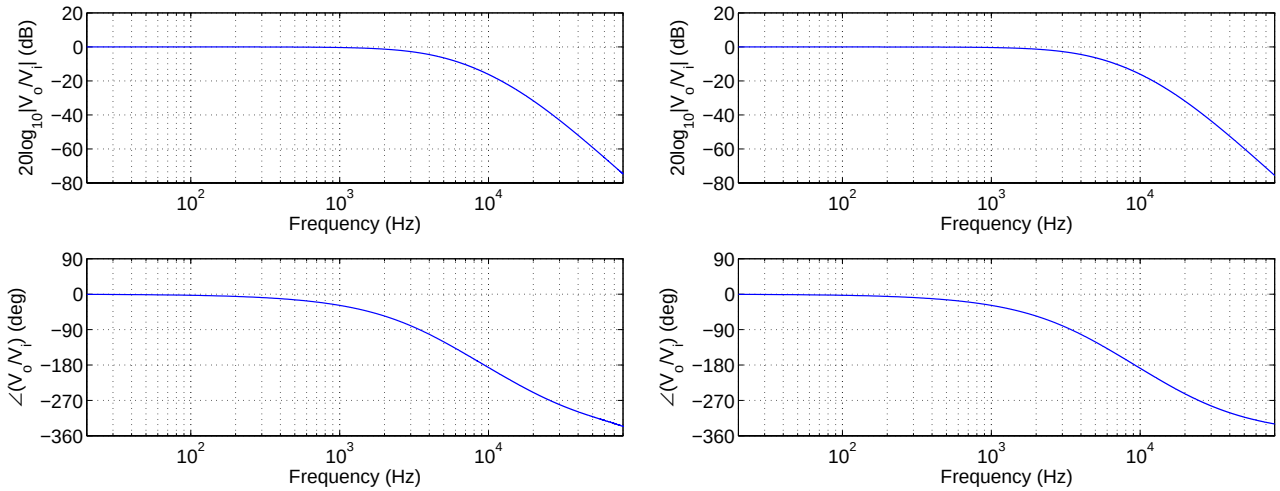

Fig. 19: Amplitude (top plots) and phase (bottom plots) of the frequency response function of the cascade of two low pass filters: measured frequency response function (left hand side) and simulated frequency response function (right hand side).

In order to avoid noise effects at low frequencies, two Sallen-Key high pass filters [9] of the second order with cut off frequencies at about 10 Hz have been placed in cascade to the low pass filters. A scheme of a Sallen-Key second order high pass filter is shown in Figure below.

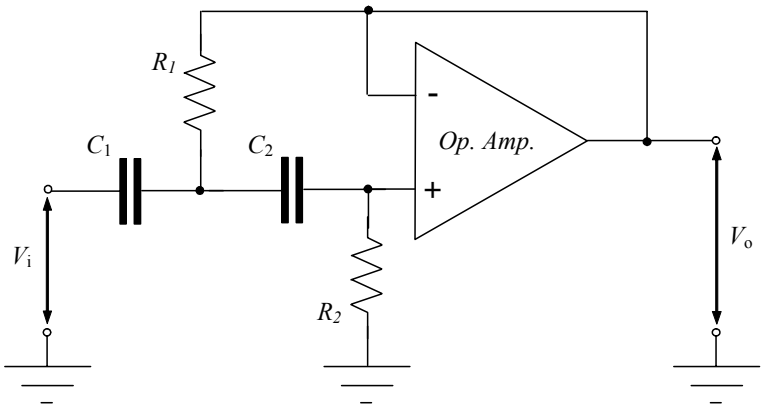

Fig. 20: Electrical scheme of a second order Sallen-Key high pass filter circuit.

The frequency response function of this filter is given by:

$$\frac{V_o}{V_i} = \frac{-\omega^2\omega_0^2}{-\omega^2 + j\omega\left(\frac{1}{R_2C_1} + \frac{1}{R_2C_2}\right) + \omega_0^2}. \tag{3.1.4}$$

The cut off frequency is again given by Equation 3.1.3. Tables 8 and 9 summarise the electric components of the two filters respectively.

Table 8: Values of the electrical elements for the first high pass filter circuit.

Parameter	Value
Operational amplifier	OPA131
R_1	5.23 kΩ
R_2	10.5 kΩ
C_1	4.7 μF
C_2	1.0 μF
f_c	9.906 Hz

Table 9: Values of the electrical elements for the second high pass filter circuit.

Parameter	Value
Operational amplifier	OPA131
R_1	2.15 kΩ
R_2	25.5 kΩ
C_1	4.7 μF
C_2	1.0 μF
f_c	9.915 Hz

Figure 21 shows the comparison between the simulated and the measured frequency response functions of the cascade of the two high pass filters. In this case the low-frequency amplitude reduction of the response is about 24 dB/octave but the analogue circuit leads the phase of +360°.

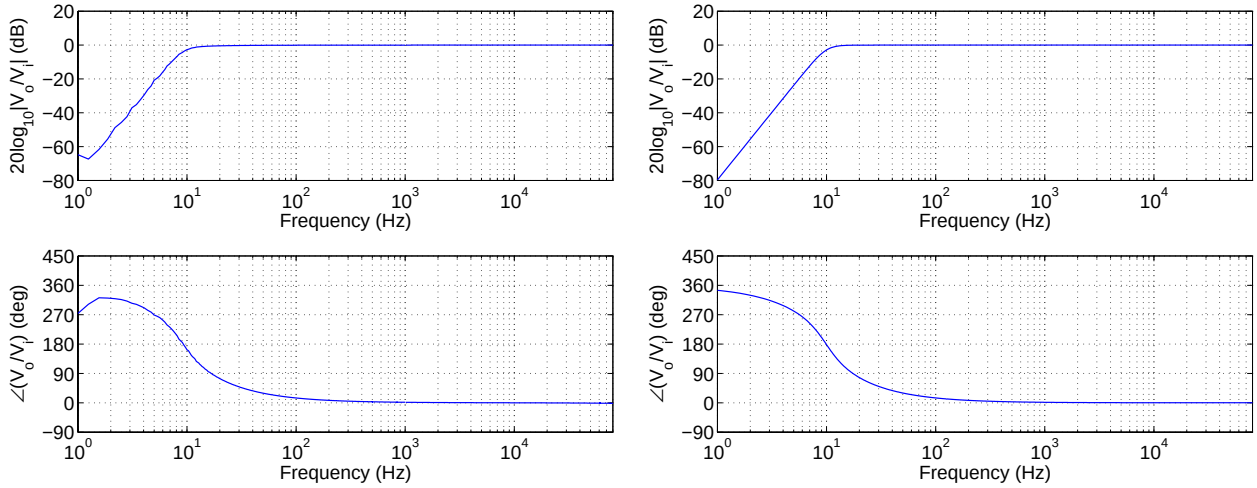

Fig. 21: Amplitude (top plots) and phase (bottom plots) of the frequency response function of the two high pass filter: measured frequency response function (left hand side) and simulated frequency response function (right hand side).

In conclusion, the compensator, built in order to improve the stability of the control unit, is made of a cascade of two second order low pass filters with cut off frequencies at 5.305 kHz and 15.915 kHz respectively and two high pass filters with cut off frequencies at about 10 Hz. The measured and the simulated frequency response functions of the complete control chain (filters-amplifier-integrator) are shown in Figure 22.

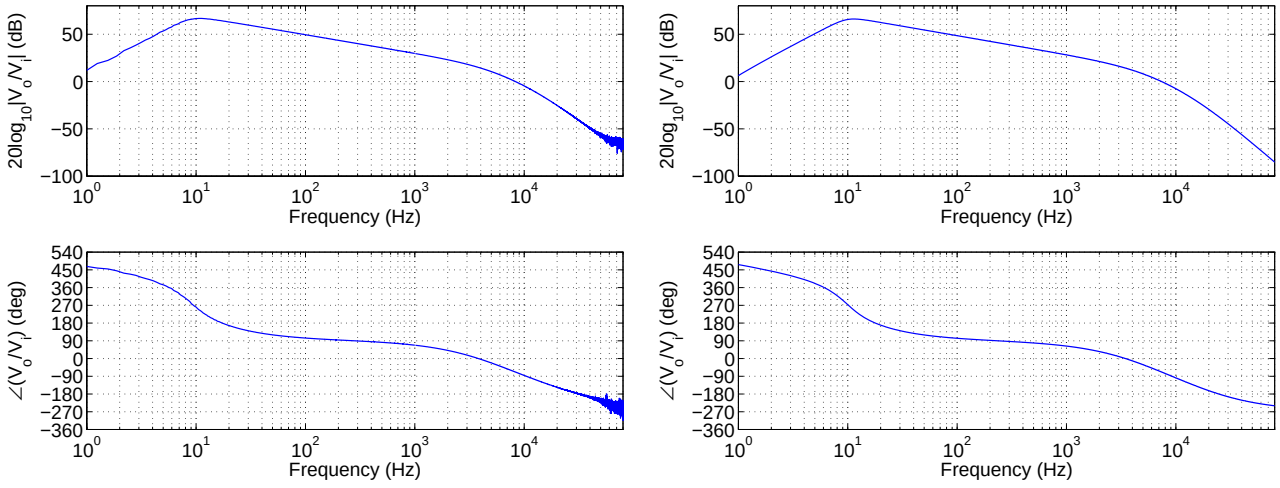

Fig. 22: Amplitude (top plots) and phase (bottom plots) of the frequency response function of the compensator: measured frequency response function (left hand side) and simulated frequency response function (right hand side).

The Bode plots highlight that the mathematical models used in order to design the electric commponents of the controller are in good agreement with the real behaviour of the analogue

circuits. For frequencies higher than 60 kHz the response becomes very low and therefore it s heavily affected by floor noise.

The scheme in Figure 23 shows the complete measurement chain with the sensor-actuator transducers, compensator, integrator and amplifier components. Figure 24 shows the Bode and the Nyquist plots of the open loop FRF between the output signal v of the analogue integrator with the analogue compensator in cascade and the input signal u_i to the high voltage amplifier which drives the piezoelectric patch actuator bonded at the control position number 2 on the panel.

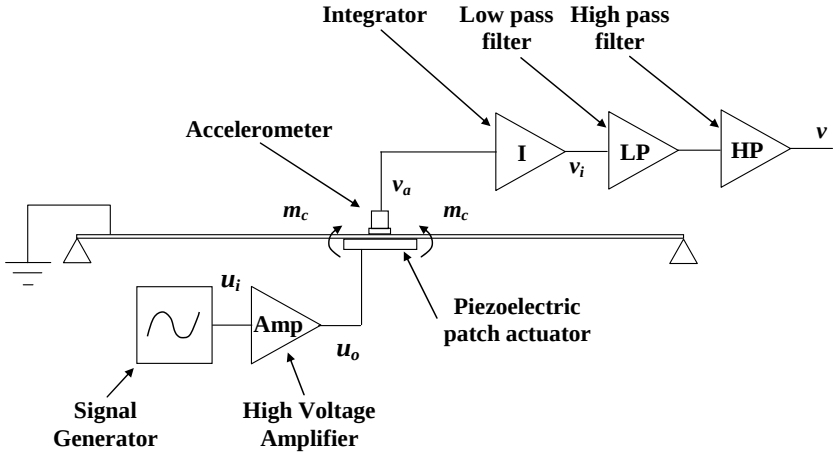

Fig. 23 Aluminium plate excited in bending by a piezoelectric patch strain actuator bonded to the plate. The actuator is driven by the output signal u_o of an high voltage amplifier and the transverse velocity v of the plate is measured by an accelerometer sensor with an analogue integrator circuit and a compensator in cascade.

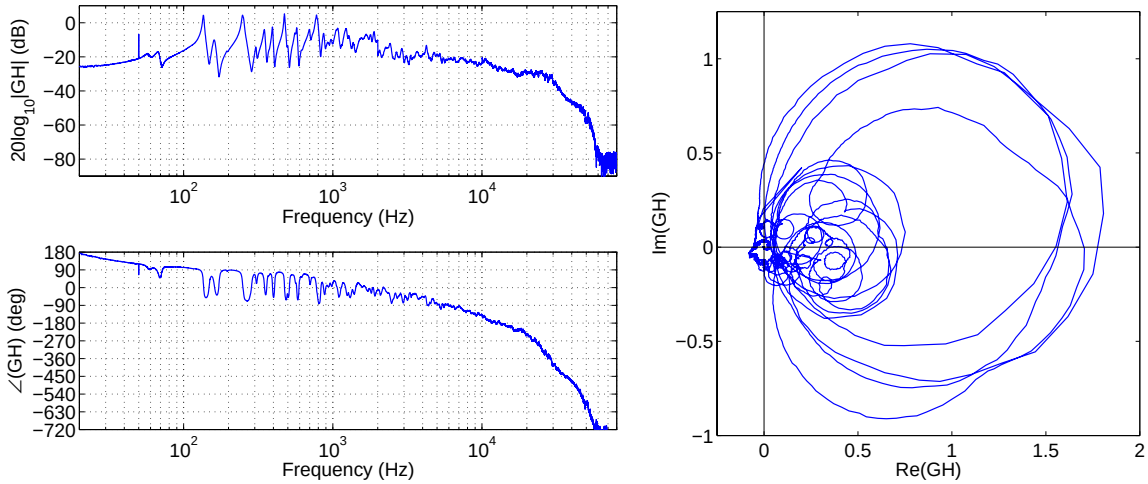

Fig. 24: Bode plot (left hand side) and Nyquist plot (right hand side) of the open loop frequency response function between the output signal of an accelerometer sensor with the analogue integrator and the analogue compensator in cascade and the input signal to the high voltage amplifier which drives the piezoelectric patch strain actuator attached at the control position number 2 on the panel.

In comparison to the open loop FRF without the analogue controller (see Figure 17) the phase exceeds -90° at about 6 kHz because of the phase lag due to the first of the two low pass filters. At the same time, for frequencies higher than 6 kHz, the amplitude response is diminished by 35-40 dB. In this way, as shown by the Nyquist plot, the real negative part of the sensor-actuator open loop

FRF which is responsible for the conditional stability and loss of control performance of the feedback loop, has been reduced. The control unit is still only conditionally stable, but now the real positive part of the FRF locus is much bigger than the negative real part. Thus it is possible to implement larger feedback control gains which produce greater vibration reductions at the error positions. Moreover the maximum control gain itself is increased greatly.

3.2 Stability analysis and design of five decentralised control units

In order to assess the stability of the decentralised multi channel control system, it is necessary to study the stability of the five control units simultaneously. The block diagram of the five channels control system is shown in Figure 25.

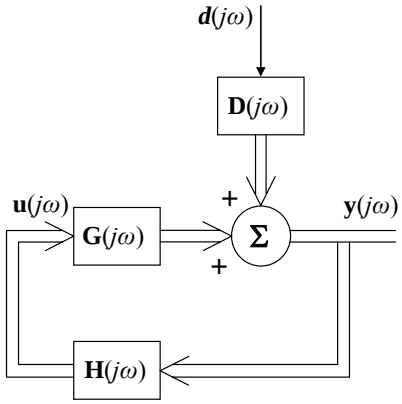

Fig. 25: Block diagram of a multi channel direct velocity feedback (DVFB) control system.

In this case, the vector with the error sensor signals $\mathbf{y}(j\omega)$ is given by:

$$\mathbf{y}(j\omega) = \left[\mathbf{I} + \mathbf{G}(j\omega)\mathbf{H}(j\omega)\right]^{-1} \mathbf{D}(j\omega)d(j\omega), \tag{3.2.1}$$

where $\mathbf{D}(j\omega)$ is a column vector with the FRFs between the sensors and the primary source $d(j\omega)$, $\mathbf{G}(j\omega)$ is a 5×5 square matrix whose elements are the open loop FRFs between the sensors and the actuators. For example the first column of $\mathbf{G}(j\omega)$ is given by the FRFs between the five accelerometers output signals and the input signal to the piezoelectric actuator in the control position number 1. $\mathbf{H}(j\omega)$ is a 5×5 diagonal square matrix whose elements on the diagonal are given by the FRFs of the analogue controllers (integrators, compensators, amplifier).

In order to analyse the stability of the MIMO control system, the locus of the five eigenvalues of the matrix $\mathbf{G}(j\omega)\mathbf{H}(j\omega)$ has been studied [12]. The system is stable if the locus does not encircle the Nyquist point (-1+j0) when the circular frequency ω goes from $-\infty$ to $+\infty$. In order to build the

matrix $\mathbf{G}(j\omega)\mathbf{H}(j\omega)$, twenty five FRFs have been measured in a frequency range between 20 Hz and 80 kHz.

Figures 26 and 27 show respectively the amplitudes and the phases of the twenty five open loop frequency response functions. For example rows number 1 in the two plots show the open loop amplitudes and phases at the five accelerometer sensors when the piezoelectric actuator in the position number 1 excites the structure. Comparing the diagonal plots with the off diagonal plots in Figure 27, the phase lag induced by the distance between the excitation source position and the measurement positions can be noticed.

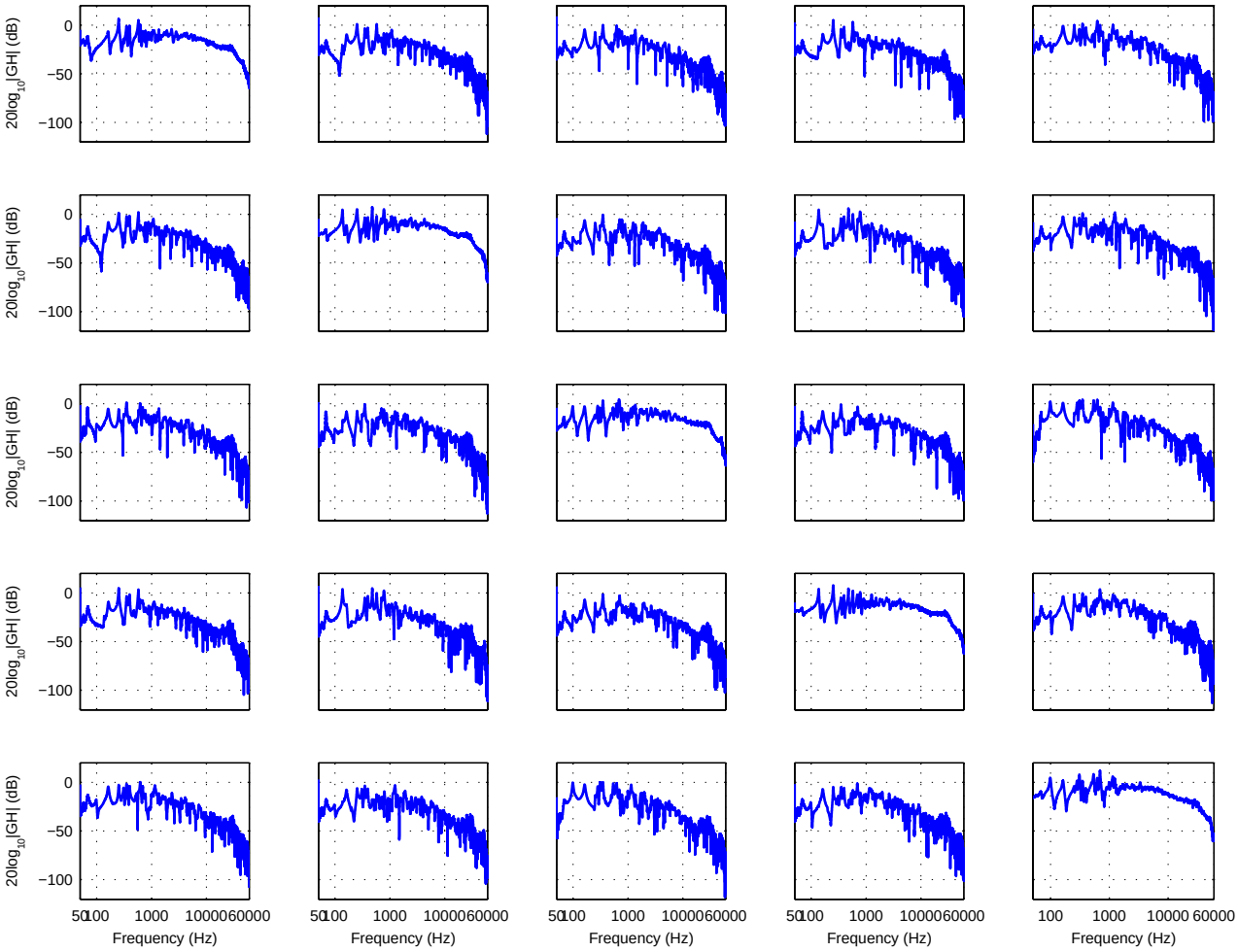

Fig. 26: Amplitudes of the 5×5 matrix of sensor-actuator open loop FRFs.

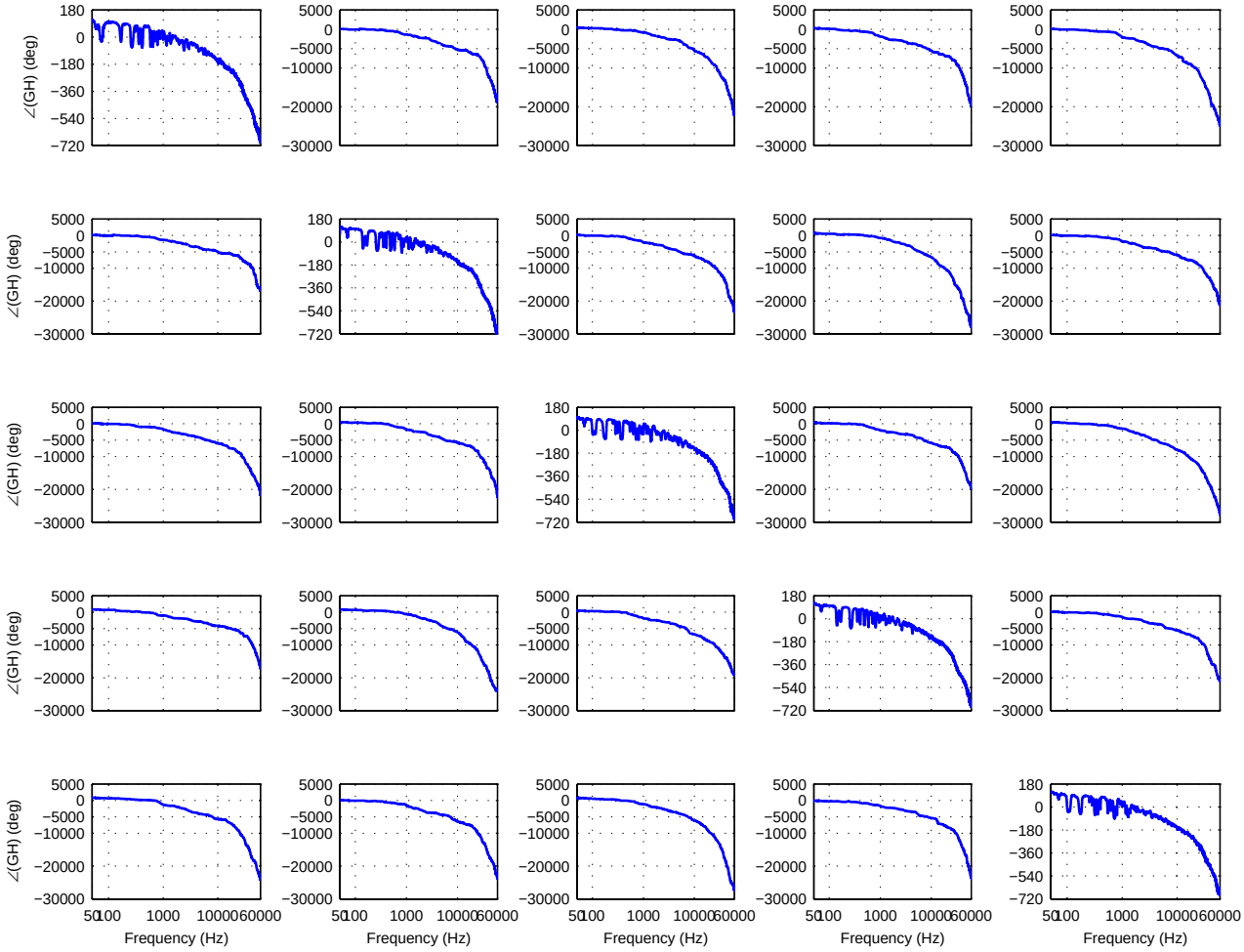

Fig. 27: Phases of the 5×5 matrix of sensor-actuator open loop FRFs.

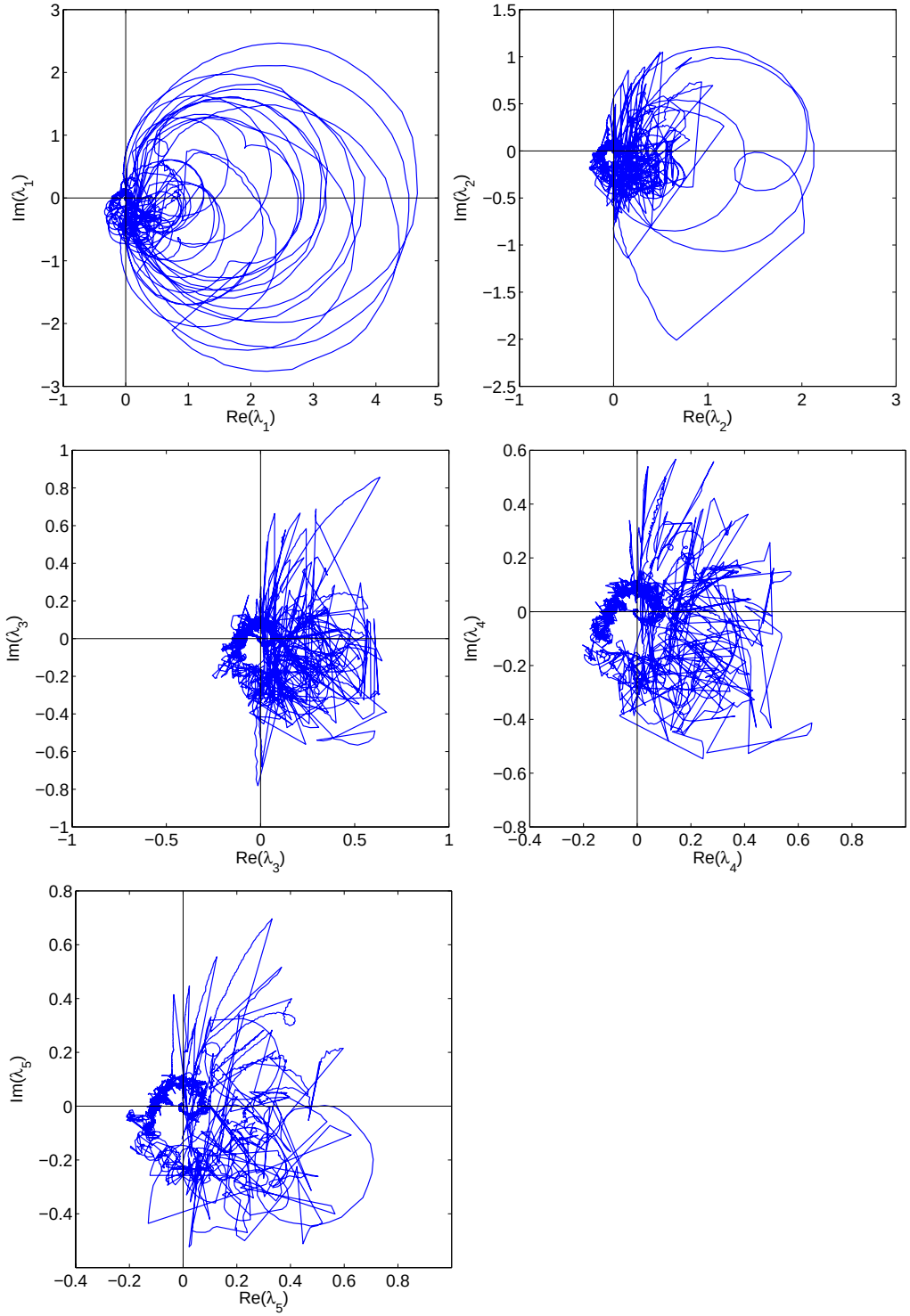

Fig. 28: Nyquist plots in the 20 Hz-80 kHz frequency range of the locus of the five eigenvalues of the system.

Figure 28 shows the loci of the five eigenvalues of the matrix $\mathbf{G}(j\omega)\mathbf{H}(j\omega)$. All eigenvalues loci encircles the Nyquist point. Thus the five channels system is conditional stable. Also the maximum control gains that enable stable feedback control loops are lower than those found for the five single channel feedback control loops acting in isolation.

4. IMPLEMENTATION OF FIVE DECENTRALISED DVFB CONTROL UNITS

In this Section, the performances of the smart panel with five decentralised control units designed and built for this study are analyzed. At first the vibrations reduction at error position number 2, when only the corresponding control loop is closed, will be introduced. Subsequently the vibration reductions at all error positions when all control loops are implemented with suitable gains will be described. Finally the sound reduction achieved by the five control loops is presented.

4.1 Vibrations at the error positions

In the last Section the stability of a single feedback control loop and of the multi channel decentralised feedback control system has been assessed. In order to study the performances of the control system, the smart panel has been mounted on the test facility described in Subsection 2.5. As shown in Figure 29, five feedback control loops have been implemented. The panel has been excited by a point force generated by a shaker.

Figure 30 shows the amplitude of the frequency response function between the output signal of the accelerometer at the error position number 2, v_{e2}, with an ideal integrator and the primary excitation, F_p, generated by the shaker.

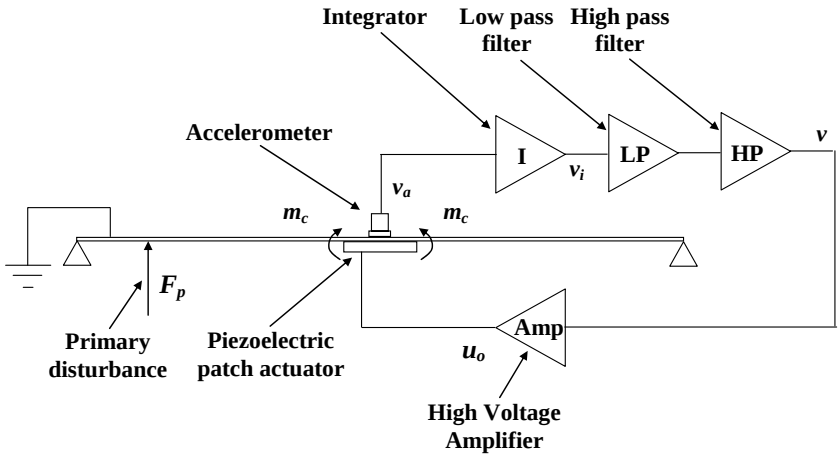

Fig. 29 Scheme of the five feedback control loops implemented in the final control performance tests.

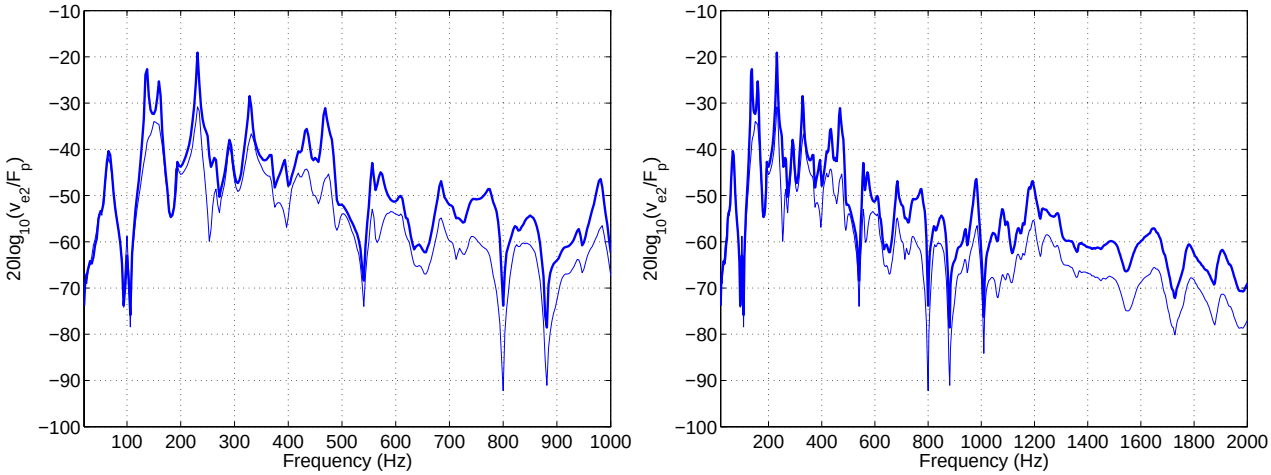

Fig. 30: Amplitude of the frequency response function between the output signal of the accelerometer sensor number 2 with the ideal integrator and the force transmitted by a shaker to the panel in the 20 Hz-1 kHz frequency range (left hand side) and in the 20 Hz-2kHz frequency range (right hand side). Solid line without control, faint line with control.

The solid line represents the response function when the feedback control channel number 2 is turned off while the faint line shows the response function when the feedback control is implemented with the maximum stable gain. The plots in Figure 30 highlight that the control system is able to generate reductions of the vibration at the error sensors from a minimum of about 8 dB for the second, third and sixth resonances, to a maximum of about 12 dB for the fourth and ninth resonances. Furthermore the vibrations are constantly reduced by 10 dB for frequencies higher than 1200 Hz. The use of all five decentralised control channels of the system, implemented with suitable gains, produces larger damping effects than the single control unit. Thus, as shown by the dotted line in Figure 31, at the control position 2 reductions of about 20 dB for almost all the resonances in the frequency range between 100 Hz-800 Hz are produced. Also the first and the fifth resonances, which couldn't be efficiently controlled by the feedback loop number 2, are reduced of 10 dB by the system.

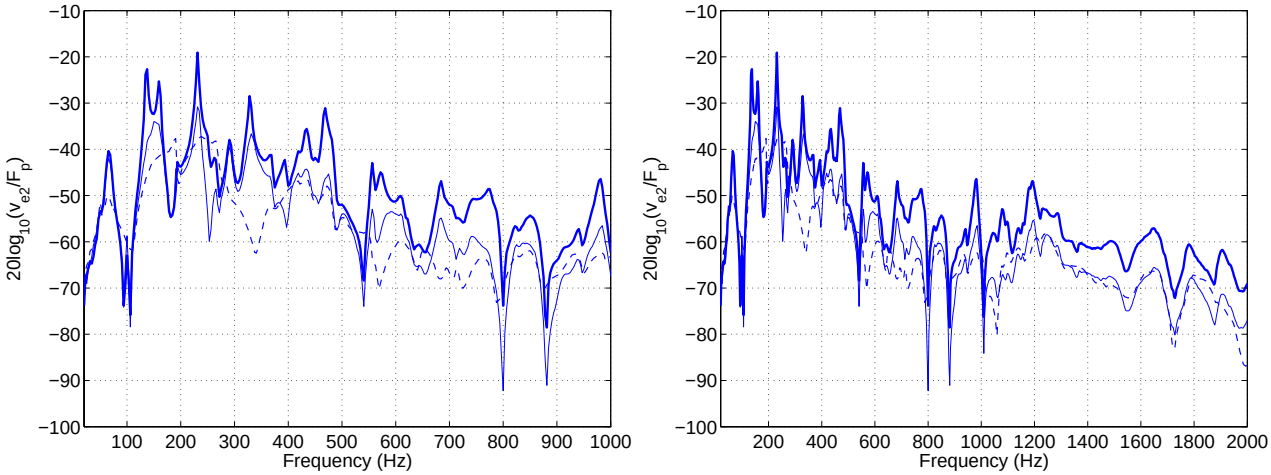

Fig. 31: Amplitude of the frequency response function between the output signal of the accelerometer sensor number 2 with the and the force transmitted by a shaker to the panel in the 20 Hz-1 kHz frequency range (left hand side) and in the 20 Hz-2kHz frequency range (right hand side). Solid line without, faint line with control.

The plots in Figure 32 below show the same analysis described for the error position 2 but extended to all five error positions of the smart panel. The analysis is performed in three frequency ranges: 20 Hz-1 kHz. 20 Hz-2 kHz and 20 Hz-5 kHz. The plots highlight that the behaviour of the other four channel is very similar to the behaviour of the control channel number 2.

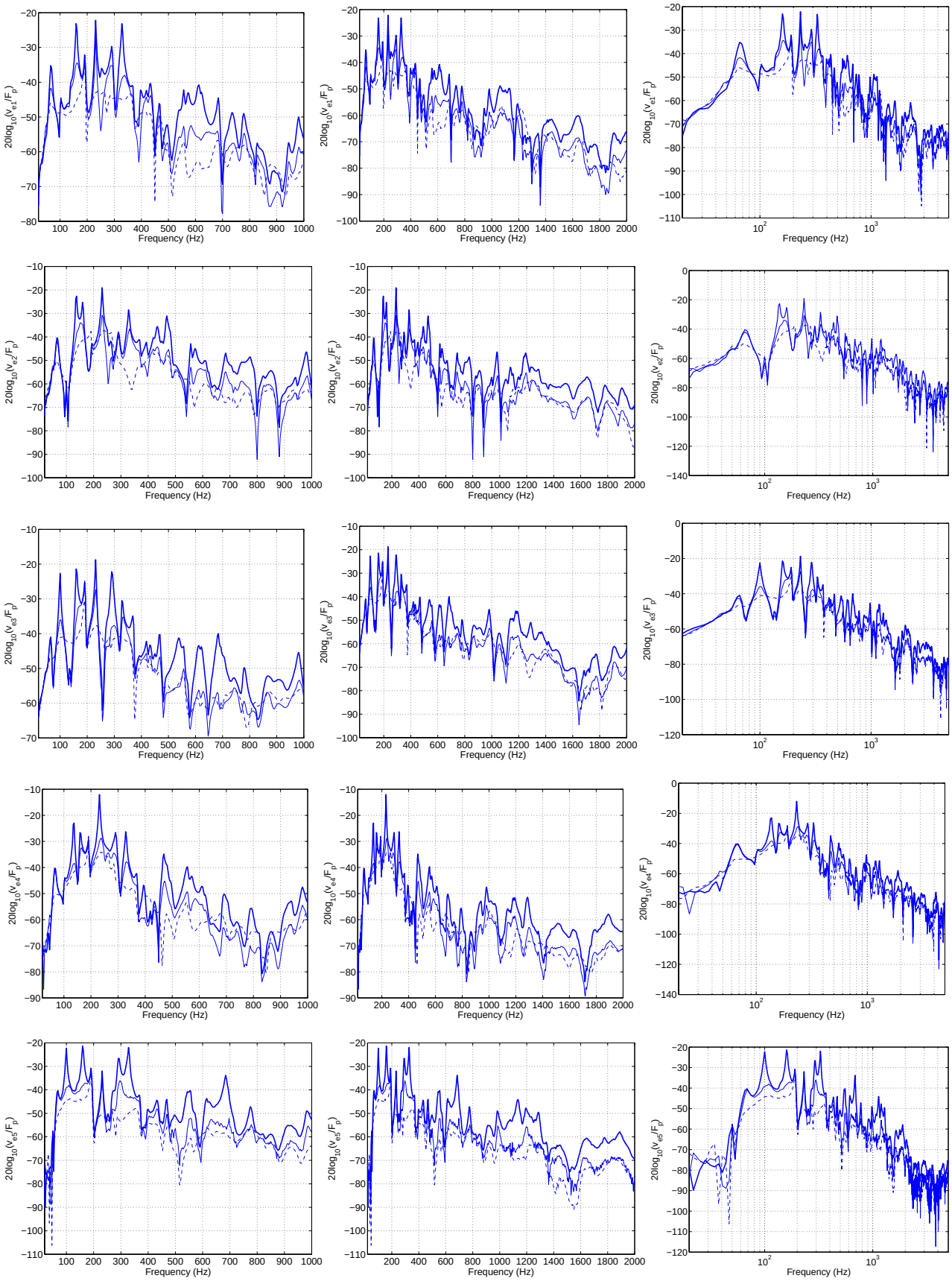

Fig. 32: Amplitude of the frequency response function between the output signal of the five accelerometer sensors with ideal integrators and the force transmitted by a shaker to the panel in the 20 Hz-1 kHz frequency range (left hand side), in the 20 Hz-2 kHz (centre) and in the 20 Hz-5kHz frequency range (right hand side). Solid line without control, faint line with the single control unit and dashed line with all five control units.

4.2 Sound pressure level

The vibration of the panel generates sound radiation. Figure 33 shows the amplitude of the frequency response function between the output signal of a microphone, P_{mic}, placed at about 0.5 m over the centre of the panel and the force transmitted by a shaker to the panel itself, F_p. The solid line shows the sound pressure without the control system and the faint line when all five decentralised feedback control systems are implemented with maximum stable gains.

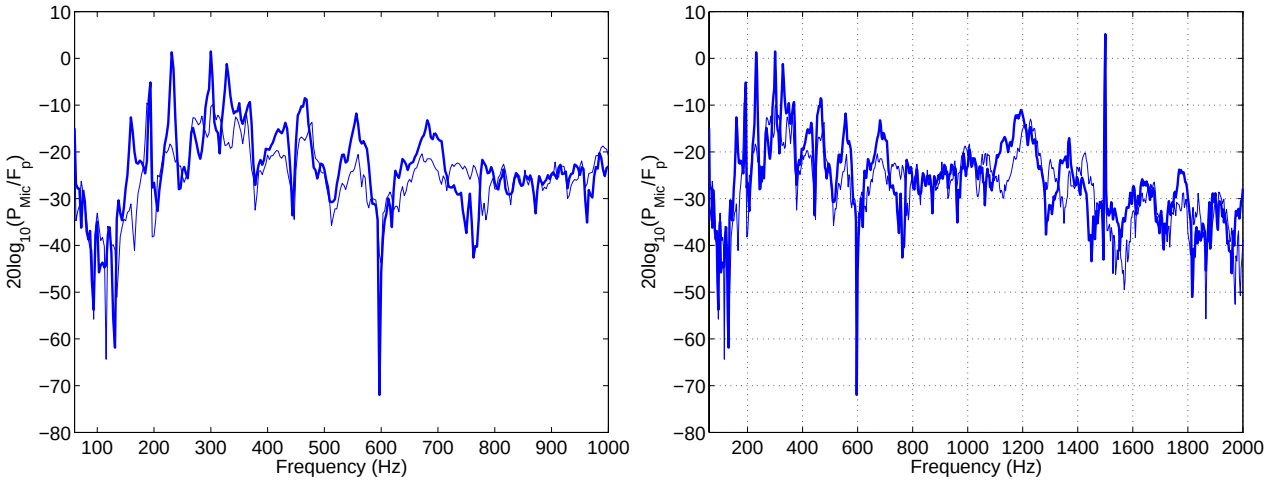

Fig. 33: Amplitude of the frequency response function between the output signal of a microphone placed at about 0.5 m over the centre of the panel and the force transmitted by a shaker to the panel in the 20 Hz-1 kHz frequency range (left hand side) and in the 20 Hz-2kHz frequency range (right hand side). The solid line represents the sound pressure when the control system is off and the faint line when all the five control loops are implemented with maximum stable gains.

The control system cuts almost all the resonances at frequencies below 700 Hz. The mean reduction is of about 8 dB, although at about 159 Hz, 231 Hz, 300 Hz and 328 Hz the reduction is about 12 dB. The plots in Figure 30 also highlight three important behaviours: the control system does not produce reduction of the resonances for frequencies higher than 700 Hz because only five control loops are implemented; at certain frequency ranges, for example between 720 Hz and 770 Hz, the control system increases the sound pressure radiated by the panel because of sound radiation spillover generated by the control system; the control system does not produce effects at a number of resonances, for example at 190 Hz, where the response of the panel is efficiently coupled with that of the cavity.

CONCLUSIONS

This Technical Report has presented the design and the construction of a smart panel with five decentralised direct velocity feedback control loops for the reduction of vibrations and of sound radiation. First the open loop frequency response function between the chosen sensor, a seismic accelerometer with in cascade an analogue integrator, and the chosen actuator, a circular piezoelectric patch strain actuator, has been studied. The analysis has highlighted that the system is only conditionally stable and that the locus of the sensor-actuator open loop FRF has comparatively equal sizes of the real positive and real negative parts. As results little control performance can be obtained. In order to improve the stability of the feedback control system a compensator, made of two low pass filters with cut off frequency at about 2 kHz and 15 kHz respectively and a high pass filter with cut off frequency at 10 Hz, has been designed and built. A new analysis of the open loop response with the controller in cascade has shown that the control system is still conditionally stable, but now the real positive part of the locus of the open loop sensor-actuator FRF is much bigger than the negative real part. In this way it has been possible to implement high control gain values in such a way as to obtain greater control effects of the panel vibrations. Before closing all the five control loops the overall stability of all the five decentralised feedback control channels has been assessed using the generalised Nyquist criterion for MIMO systems based on the measured FRF between all sensors and actuators. Finally the control performances of the smart panel has been tested using a shaker as primary disturbance and measuring the vibrations of the panel at the error positions and the sound pressure at about 0.5 m over the centre of the panel. The implementation of the five control channels has produced the following results.

- The transverse velocity of the plate in correspondence to the five error sensors is reduced by about 20 dB in the frequency range between 100 Hz and 800 Hz. The control performance is good also for frequencies higher than 800 Hz and the vibration reduction is of about 8-10 dB.
- At certain frequencies, for example 190 Hz, the control system is not able to reduce the vibrations of the panel. Probably at these frequencies the response of the cavity is well coupled to that of the panel.
- The control system is able to achieve good reductions of the sound radiated by the panel. In particular the control system cuts almost all the resonances at frequencies below 700 Hz. The mean reduction is of about 8 dB but at certain frequencies, for example 231 Hz and 300 Hz, the reduction is between 12dB and 15 dB.
- The control system is not able to control the sound radiation for frequencies higher than 700 Hz. This fact is probably due to the low number of decentralised control channel on the panel.

AKNOWLEDGEMENTS

Part of this project has been carried out within the “Laboratorio di Acustica e Vibrazioni” which is supported by Regione Emilia Romagna - Assessorato Attività Produttive, Sviluppo Economico, Piano telematico, PRRIITT misura 3.4 azione A - Fondi Obiettivo 2 (I). Also, the piezoelectric patch actuators used for the parametric study presented in the appendix have been fabricated at the “Instituto di Scienza e Tecnologia dei Materiali Ceramici” of Faenza (I).

REFERENCES

[1] S.J. Elliott, P. Gardonio, T.C. Sors and M.J. Brennan, 2001 Active vibro-acoustic control with multiple feedback loops, *Journal of the Acoustical Society of America*, Vol. 111, No. 2, pp. 908-915.

[2] P. Gardonio, E. Bianchi and S.J. Elliott. Smart panel with multiple decentralized units for the control of sound transmission. Part I: theoretical predictions. Part II: design of the decentralised control units. Part III: control system implementation. *Journal of Sound and Vibration*, **274**, 163-192, 193-213, 215-232.

[3] A. Preumont, 2002 *Vibration control of active structures.* (London: Kluwer Academic Publihers, 2nd Edition).

[4] J.Q. Sun, 1996 Some observations on physical duality and collocation of structural control sensors and actuators, *Journal of Sound and Vibration*, Vol. 194, pp. 765-770.

[5] G. Marro, 1987 *Controlli Automatici* (Bologna, Zanichelli, 3rd Edition)

[6] G.F. Franklin, J.D. Powell and A. Emami-Naeini, 2002 *Feedback control of dynamic systems.* (Prentice Hall, 4th Edition).

[7] M.J. Brennan, S.J. Elliott and R.J. Pinnington, 1997 The dynamic coupling between piezoceramic actuators and a beam, *Journal of the Acoustical Society of America*, Vol. 102, No. 4, pp. 1931-1942.

[8] Y. Aoki, P. Gardonio and S.J. Elliott, 2006 Stability of a Piezoelectric Patch-Accelerometer Active Damping Control System in Smart Panel. *Euronoise 2006*, Tampere, Finland, 30 May – 1st June 2006.

[9] R. Libbey. 1991 *Handbook of circuit mathematics for technical engineers* (Boca Raton CRC)

[10] M. Gavagni, P. Gardonio and S. J. Elliott, 2004, Theoretical study of a velometer sensor-piezoelectric patch actuator pair for direct velocity feedback control systems. *ISVR Technical Report* No 303

[11] S.S. Rao 1995 *Mechanical Vibration.* (New York: Addison-Wesley Publishing Company, 3rd Edition).

[12] S. J. Elliott S.J. Elliott, 2001 *Signal Processing for Active Control*, Academic Press, London.

APPENDIX 1

Parametric study of piezoelectric patch actuator

As discussed in Subsection 2.2, the piezoelectric patch actuators, used in the five feedback control loops, have been chosen on the base of the results of a parametric study. The study has been carried out using a large number of piezoelectric patch actuators bonded to an aluminium plate (see Figure 34 below) similar to the one used to build the smart panel considered in this Report.

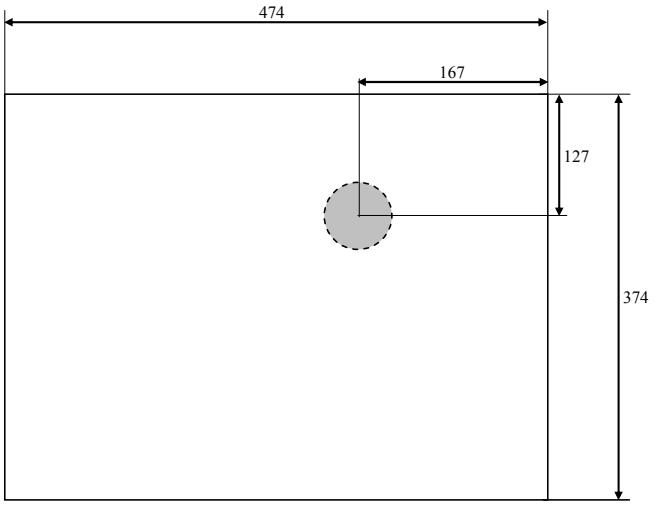

Fig. 34 Aluminium panel with a piezoelectric patch actuator. The actuator, represented by the grey circle, is attached on the bottom of the plate. The positions of the actuator and the dimensions of the plate are expressed in mm.

Figure 35 shows the experimental setup used to measure the frequency response function between the transverse velocity, v_v of the plate and the input voltage, u_o, to the piezoelectric patch actuator bonded to the plate. As shown in Figure 35, the transverse velocity of the plate is measured by a laser vibrometer and the input voltage u_o is the output signal of a high voltage amplifier. Thus the dynamics of a practical sensor and of the high voltage amplifier are left out from the measurement chain. A white noise signal in the 20-90 kHz frequency range, drives the high voltage amplifier.

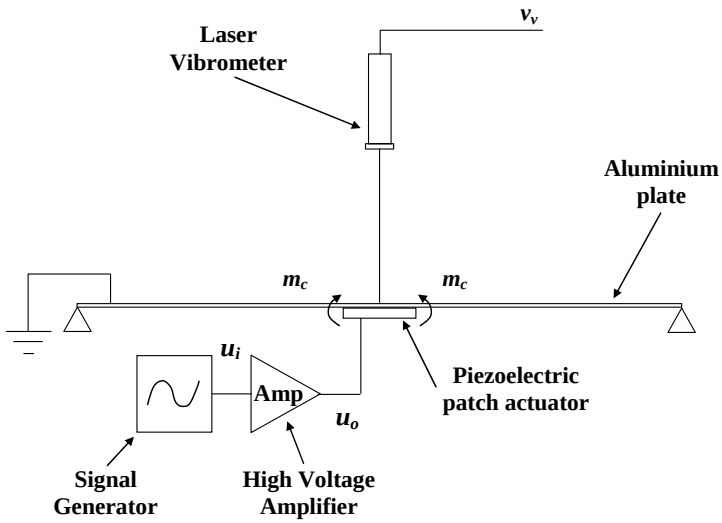

Fig. 35 Aluminium plate excited in bending by a piezoelectric patch strain actuator bonded to the plate. The actuator is driven by the output signal, u_o, of an high voltage amplifier and the transverse velocity, v_v, of the plate is measured by a laser vibrometer.

In order to investigate the influence of shape, dimensions and mass on the sensor-actuator FRF, the piezoelectric patch actuator samples have been divided in two groups. In the first group piezoelectric patch actuators of different shape (squared, circular and rectangular), different dimensions, same thickness and different masses have been considered. The characteristics of the samples belonging to this group are summarised in Table 10 below and the physical properties of the piezoelectric material are summarised in Table 2.

Table 10: Properties of the piezoelectric patch actuator samples belonging to the first group.

Type	Length/Diameter [mm]	Width [mm]	Thichness [mm]	Mass [g]
St1	10.00	10.00	1.00	0.765
St2	20.00	20.00	1.00	3.060
St3	30.00	30.00	1.00	6.885
St4	40.00	40.00	1.00	12.240
Ct1	9.00		1.00	0.480
Ct2	13.00		1.00	1.015
Ct3	17.00		1.00	1.736
Ct4	25.00		1.00	3.755
Rt1	12.00	8.00	1.00	0.734
Rt2	24.00	16.00	1.00	2.937
Rt3	37.00	24.00	1.00	6.793
Rt4	44.00	32.00	1.00	10.771

The capital letters “S”, “C”, and “R” in the acronym of the samples indicate the type of shape (squared, circular and rectangular respectively) while the letter “t” indicates that the samples have constant thickness. Figures 36, 37 and 38 show the Bode and the Nyquist plots of the sensor-actuator FRF for the samples with squared shape, circular shape and rectangular shape respectively, all of them with constant thickness.

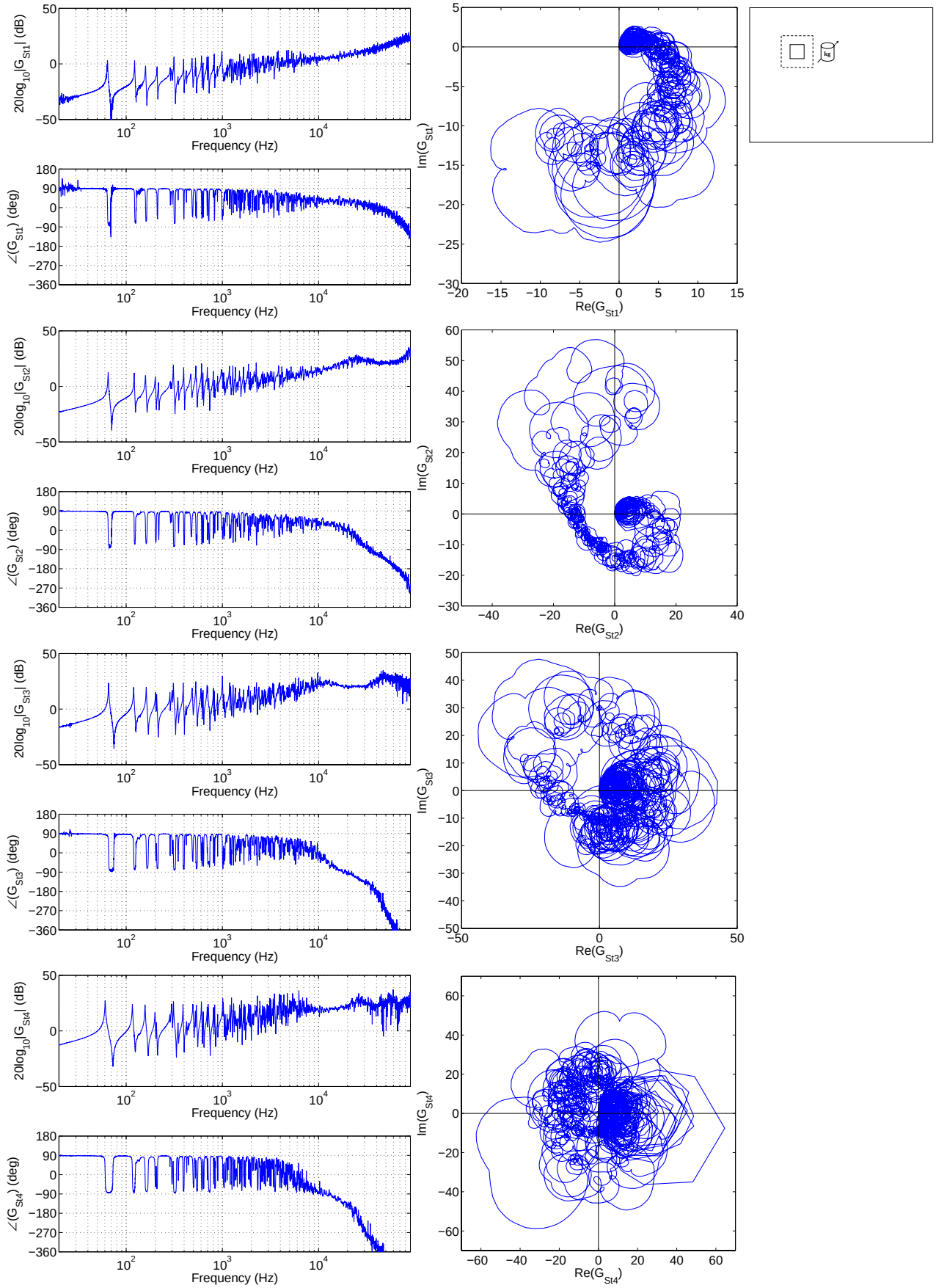

Fig. 36: Bode plots (left hand side) and Nyquist plots (right hand side) of the frequency response function between the output signal of a laser vibrometer, v_v, and the output signal of an high voltage amplifier, u_o, which drives the piezoelectric patch actuators with squared shape and constant thickness St1, St2, St3 and St4.

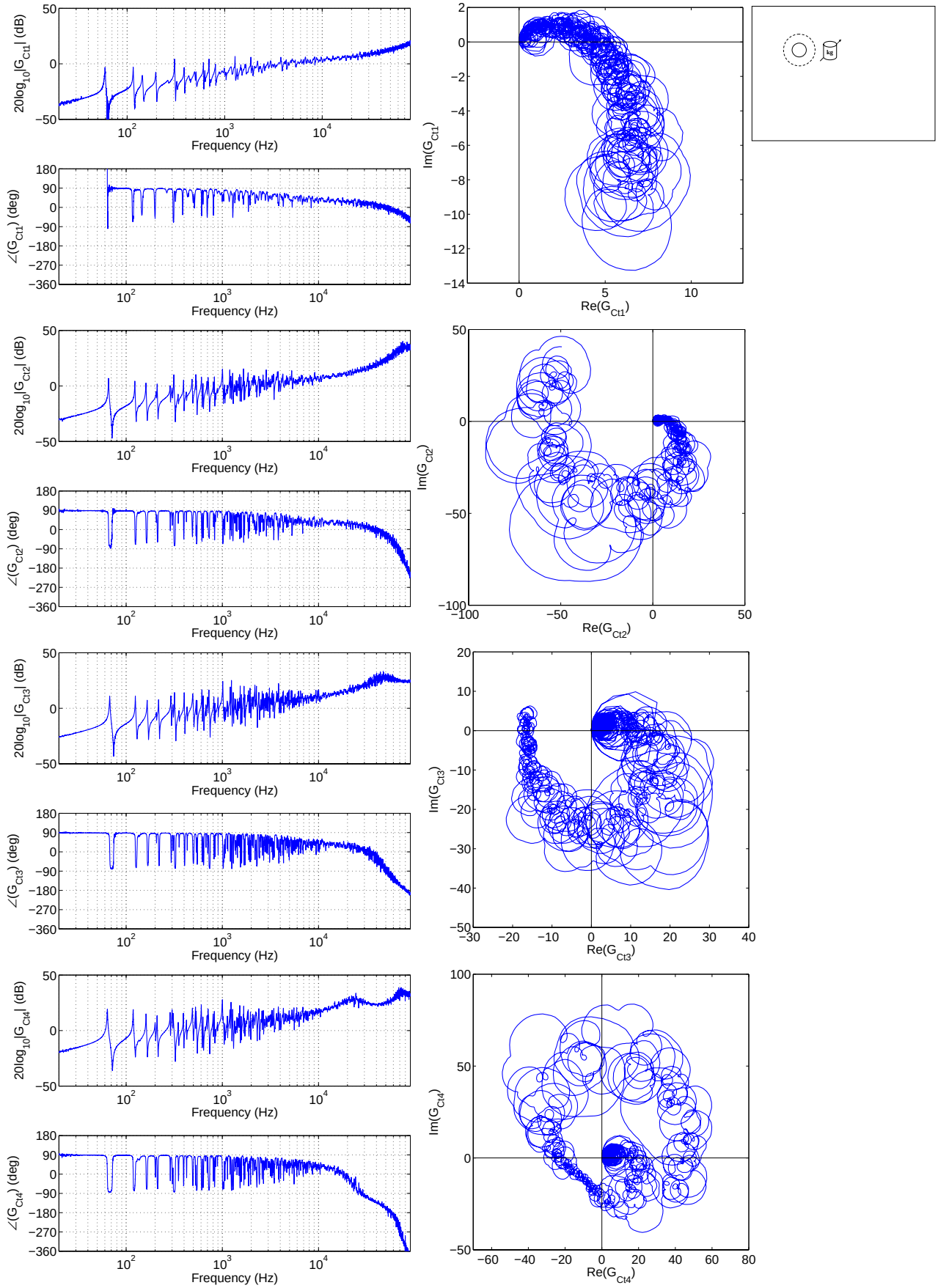

Fig. 37: Bodes plot (left hand side) and Nyquist plots (right hand side) of the frequency response function between the output signal of a laser vibrometer, v_v, and the output signal of an high voltage amplifier, u_o, which drives the piezoelectric patch actuators of circular shape and constant thickness Ct1, Ct2, Ct3 and Ct4.

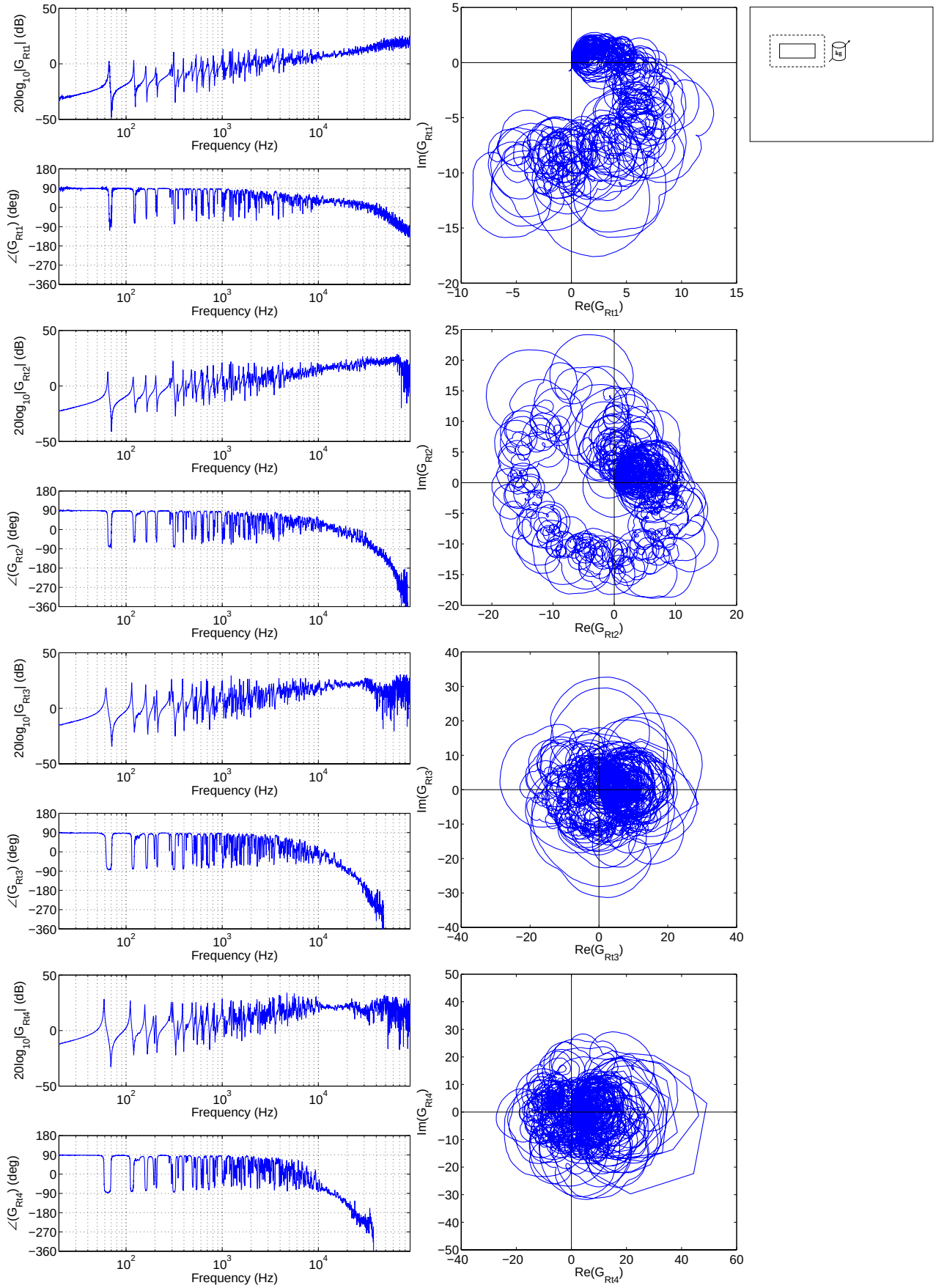

Fig. 38: Bode plots (left hand side) and Nyquist plots (right hand side) of the frequency response function between the output signal of a laser vibrometer, v_v, and the output signal of an high voltage amplifier, u_o, which drives the piezoelectric patch actuators with rectangular shape and constant thickness Rt1, Rt2, Rt3 and Rt4.

The Bode plots show that the piezoelectric patch actuators excite the panel more efficiently at high frequencies but at the same time the phase rolls off monotonically with the frequency. Moreover the Bode plots highlight other two important features: first, the amplitude of the frequency response function increases when the dimensions of the samples increase, this is because the bending moments generated by the piezoelectric actuator along its edges are proportional to the dimensions of the actuator; second, the phase roll off increases when the dimensions of the actuators increase. This feature is due to the fact that bigger is the size of the actuator, smaller is the collocation between sensor and actuator.

The Nyquist plots highlight that the vibrometer sensor-piezoelectric patch actuator system is characterised by an intrinsic instability. This instability is partially reduced by using the circular actuator.

In the second group piezoelectric patch actuators of different shapes (squared, circular and rectangular), different dimensions, different thicknesses and same mass have been considered. The characteristics of the samples belonging to this group are summarised in Table 11 below and the physical properties of the piezoelectric material are summarised in Table 2.

Table 11: Properties of the piezoelectric patch actuator samples belonging to the second group.

Type	Length/Diameter [mm]	Width [mm]	Thichness [mm]	Mass [g]
Sm1	15.00	15.00	2.90	5.00
Sm2	20.00	20.00	1.63	5.00
Sm3	25.00	25.00	1.05	5.00
Cm1	9.00		2.71	5.00
Cm2	10.25		2.86	5.00
Cm3	12.72		1.29	5.00
Rm1	18.00	12.00	3.03	5.00
Rm2	24.00	16.00	1.70	5.00
Rm3	30.00	20.00	1.09	5.00

Again, the capital letters “S”, “C”, and “R” in the acronim of the sample indicate the type of shape (squared, circular and rectangular respectively) while the letter “m” indicates that the samples have constant mass. Figures 39, 40 and 41 show the Bode and the Nyquist plots of the FRF between the transverse velocity of the plate and the input voltage to the actuators.

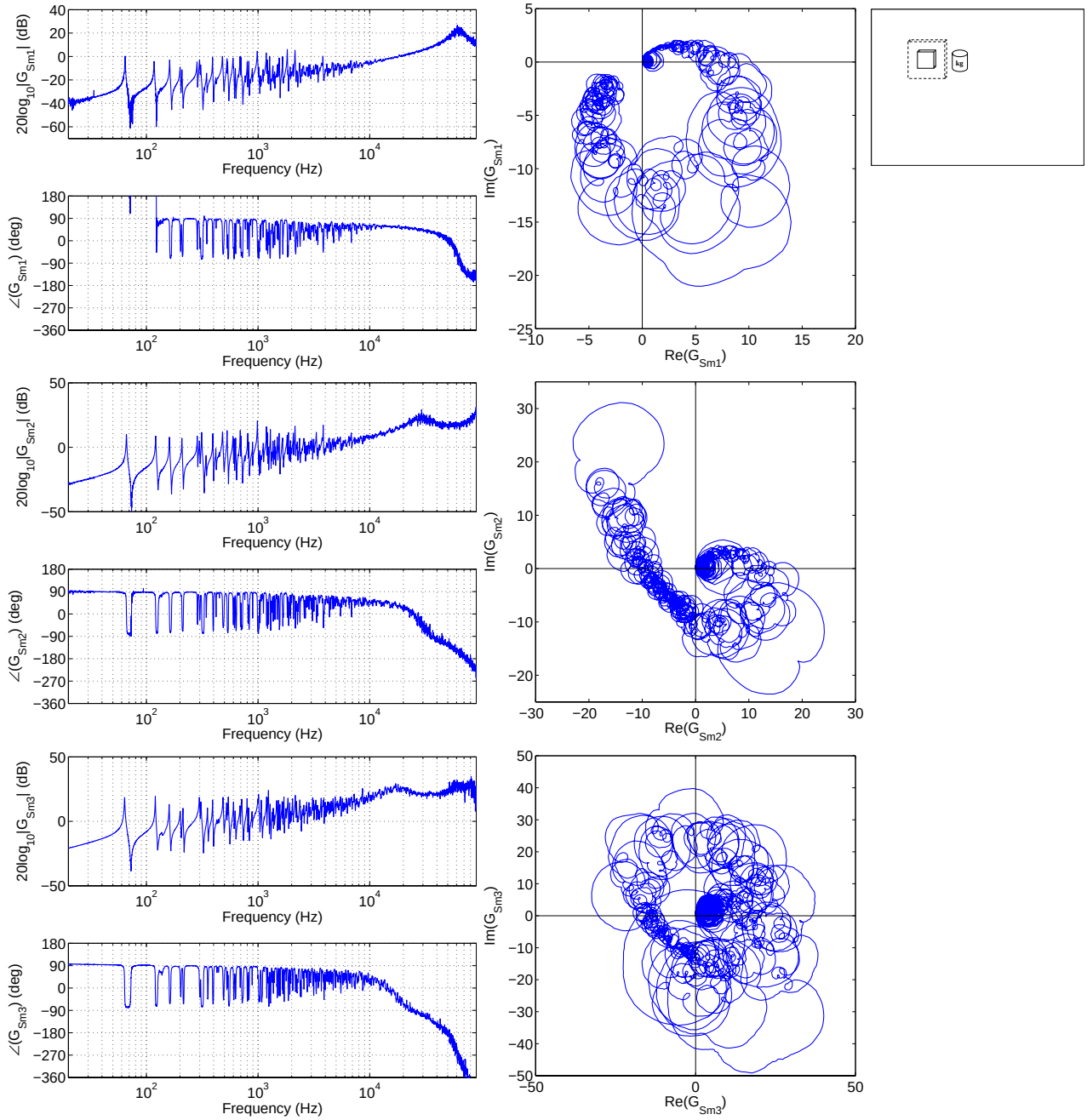

Fig. 39: Bode plots (left hand side) and Nyquist plots (right hand side) of the frequency response function between the output signal of a laser vibrometer, v_v, and the output signal of an high voltage amplifier, u_o, which drives the piezoelectric patch actuators of squared shape and constant mass Sm1, Sm2, Sm3.

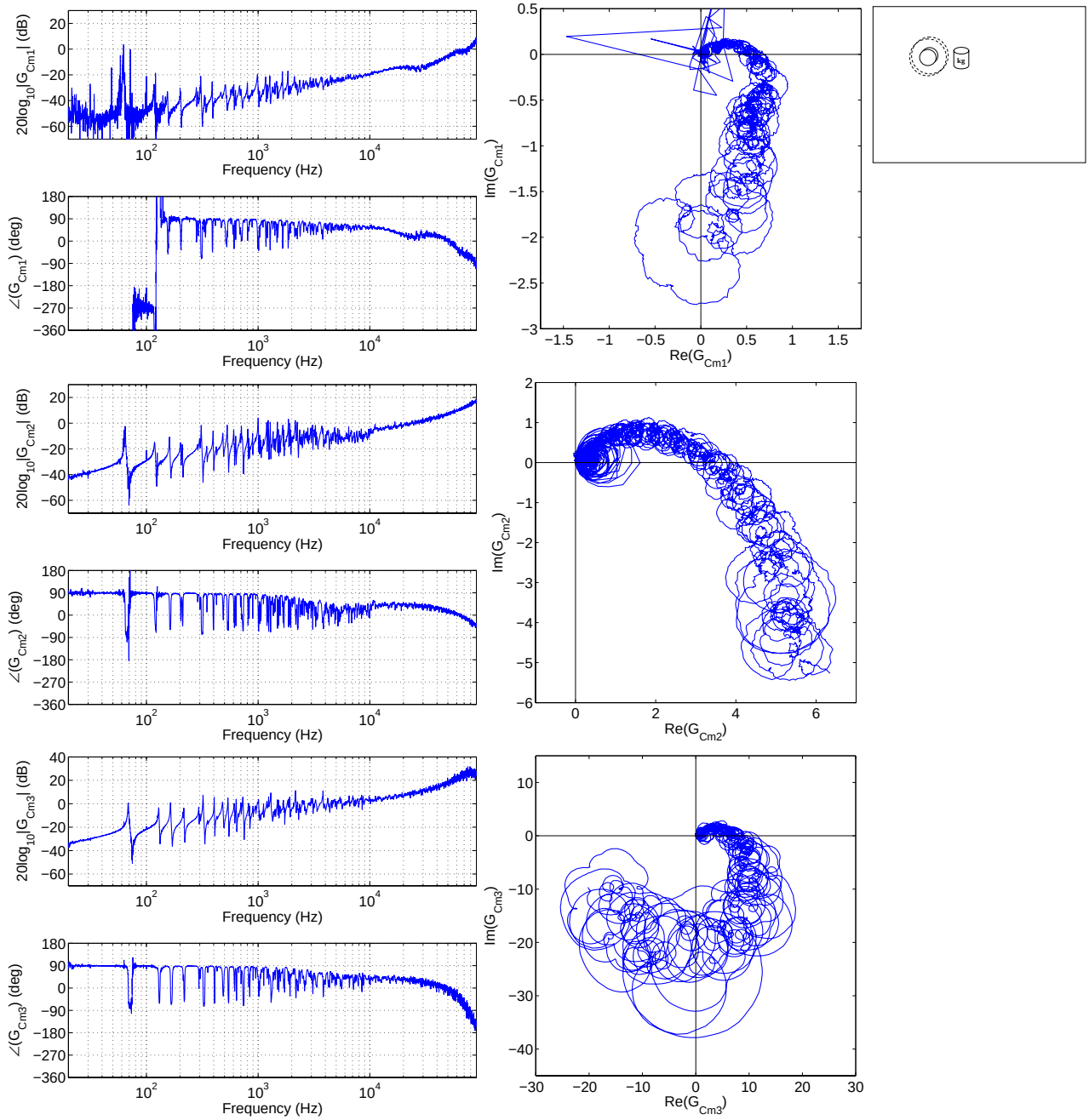

Fig. 40: Bode plots (left hand side) and Nyquist plots (right hand side) of the frequency response function between the output signal of a laser vibrometer, v_v, and the output signal of an high voltage amplifier, u_o, which drives the piezoelectric patch actuators of circular shape and constant mass Cm1, Cm2, Cm3.

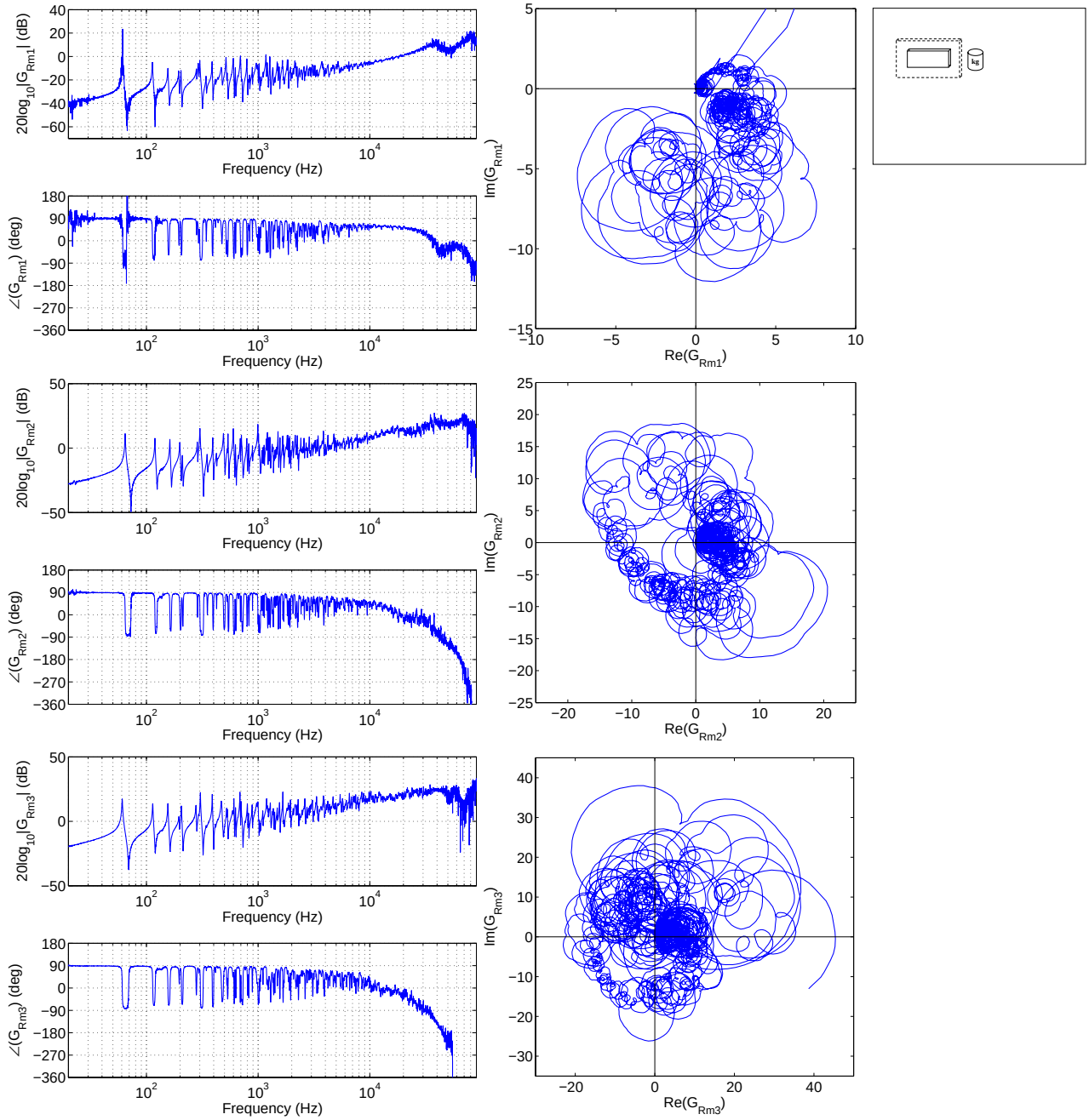

Fig. 41: Bode plots (left hand side) and Nyquist plots (right hand side) of the frequency response function between the output signal of a laser vibrometer, v_v, and the output signal of an high voltage amplifier, u_o, which drives the piezoelectric patch actuators of rectangular shape and constant mass Rm1, Rm2, Rm3.

The results obtained with these samples are similar to the results obtained with the actuator with constant thickness. Finally the parametric study has highlighted that the sensor-actuator FRF of many piezoelectric patch actuators are characterised by a wide band smooth peak. This behaviour is probably due to the dimensions of the samples but its origin is not clear.